Lithos 324–325 (2019) 152–164

Contents lists available at ScienceDirect

Lithos

journal homepage: www.elsevier.com/locate/lithos

Evidence for rutile-bearing eclogite in the mantle sources of the Cenozoic Zhejiang basalts, eastern China

Xun Yu [a], Gang Zeng [b,*], Li-Hui Chen [b], Xiao-Jun Wang [b], Jian-Qiang Liu [c], Lie-Wen Xie [d], Tao Yang [b]

[a] State Key Laboratory of Marine Geology, Tongji University, Shanghai 200092, China
[b] State Key Laboratory for Mineral Deposits Research, School of Earth Sciences and Engineering, Nanjing University, Nanjing 210023, China
[c] Institute of Marine Geology, College of Oceanography, Hohai University, Nanjing 210098, China
[d] State Key Laboratory of Lithospheric Evolution, Institute of Geology and Geophysics, Chinese Academy of Sciences, Beijing 100029, China

ARTICLE INFO

Article history:
Received 16 July 2018
Accepted 4 November 2018
Available online 07 November 2018

Keywords:
Rutile
Eclogite
Carbonated peridotite
Pacific oceanic crust
Intraplate basalts
Eastern China

ABSTRACT

Cenozoic intraplate basalts are widely distributed along the southeastern margin of Eurasia. Both carbonated and eclogitic/pyroxenitic components, which are considered related to oceanic crust recycling, have been identified in the mantle source of these basalts. However, the origin of the recycled oceanic crust and the genetic relationship between different source lithologies remain unclear. Here, we assess the source lithologies of late Miocene intraplate basalts from Ninghai, Zhejiang Province, eastern China, using new elemental and Sr–Nd–Hf isotopic compositional data. These data are also compared with those of the nearby Xinchang–Shengzhou flood basalts and other Cenozoic basalts in Zhejiang Province. New Mg isotopic compositions of the Ninghai and Xinchang–Shengzhou basalts are used to evaluate the potential influence of carbonated components during their formation. Nephelinites and basanites from Ninghai and Xinchang–Shengzhou have negative Ti and Hf anomalies, superchondritic Ca/Al ratios, and light Mg isotopic compositions ($\delta^{26}Mg = -0.35$ to $-0.38‰$), indicating a carbonated component in the mantle source. By comparison, other Ninghai basalts have positive Ti and Nb anomalies, with Sm/Yb and Lu/Hf ratios that generally correlate with Ti/Ti* values. These observations indicate that rutile-bearing eclogite should also play an important role in the formation of the Ninghai basalts, in addition to mantle peridotite. The terrestrial mantle-likeMg-isotopic compositions of the Ninghai basalts further support their formation by high-degree partial melting of such mixed source. In the plots of Sr-Nd isotopes and Ti/Ti*, the nephelinites and basanites from Ninghai and Xinchang–Shengzhou show different trends compared with other Ninghai basalts, and the carbonated component in the mantle source of the former has similar and depleted Sr-Nd isotopes to the rutile-bearing eclogite source of the latter. Additionally, samples of these basalts show negative $\Delta\varepsilon_{Hf}$ values similar to those of Pacific MORB. Subducted Pacific oceanic crust is therefore considered an appropriate source for both the carbonated and rutile-bearing eclogitic components. The Ninghai basalts provide an important insight into oceanic crust recycling in eastern China, with data indicating a genetic relationship between the carbonated component and rutile-bearing eclogite in the mantle sources of intraplate basalts.

1. Introduction

Cenozoic intraplate basalts are widely distributed in eastern China and are attributed to the recycling of subducted oceanic crust (e.g., Chen et al., 2016; Fan et al., 2014; Guo et al., 2016; Li et al., 2015; Li et al. 2016; Li et al., 2017; Liu et al., 2015; Sakuyama et al., 2013; Wang et al., 2011; Wang et al., 2015; Xu, 2014; Xu et al., 2012; Xu et al., 2017; Yang et al., 2012; Zhang et al., 2009; Zhang and Guo, 2016). Their ocean island basalt (OIB)-like trace-elemental patterns and relatively enriched radiogenic isotopic compositions indicate the existence of recycled crustal components in the mantle source (e.g., Sakuyama et al., 2013; Xu, 2014; Xu et al., 2012; Xu et al., 2017). Furthermore, geophysical observations show that the oceanic slab is stagnant in the mantle transition zone underlying the intraplate basalt area in northeast to north China (e.g., Huang and Zhao, 2006). Therefore, subducted Pacific oceanic crust is frequently considered to either directly form eclogite/eclogitic pyroxenite in the mantle source of these basalts (e.g., Li et al., 2015; Liu et al., 2015; Xu et al., 2012; Xu, 2014; Zhang and Guo, 2016) or transform into a secondary pyroxenite source during the reaction between mantle peridotite and oceanic-crust-derived SiO_2-saturated melts (e.g., Wang et al., 2011; Xu et al., 2012; Zhang et al., 2009). However, based on the enriched isotopic characteristics of some of these intraplate basalts, some studies suggest that they are more likely to originate from ancient (>1.5 Ga) recycled oceanic crust and/or sediments that were previously stored in the mantle transition zone

* Corresponding author.
E-mail address: zgang@nju.edu.cn (G. Zeng).

https://doi.org/10.1016/j.lithos.2018.11.003
0024-4937/

and then redistributed by the stagnant Pacific oceanic slab (e.g., Kuritani et al., 2011; Li et al., 2016; Liu et al., 2017a; Wang et al., 2017; Zeng et al., 2017). In addition to these mafic lithologies, carbonated components are also suggested to be widely presented in the mantle source to produce the basalts with superchondritic Zr/Hf and Ca/Al ratios, and negative Zr, Hf, and Ti anomalies (Zeng et al., 2010), which is further supported by the light Mg and heavy Zn isotopic compositions of basalts in eastern China (e.g., Li et al., 2017; Liu et al. 2016a). These carbonated components are attributed to the recycling of oceanic crust. However, the origin of the carbonated components in intraplate basalts remains debated, with both the sub-continental lithospheric mantle (e.g., Sun et al., 2017) and the mantle transition zone (e.g., Li et al., 2017) having been proposed as sources.

Intraplate basalts in southeastern China have been poorly studied due to the lack of outcrops. Carbonated components (Huang et al., 2015; Yu et al., 2015; Zeng et al., 2017) and recycled oceanic crustal materials are also proposed to present in the mantle source of the basalts. The recycled oceanic material is likely derived from either subducted Pacific oceanic crust with sediments (Li et al., 2015; Liu et al., 2016b) or ancient recycled oceanic crust (Zeng et al., 2017). Therefore, the nature of the source of Cenozoic basalts in southeastern China remains controversial. Given that the Pacific oceanic slab is thought to be stagnant in the mantle transition zone beneath the Zhejiang area (Huang and Zhao, 2006), the study of basalts from Zhejiang enables an investigation of the genetic relationship between oceanic crustal recycling and basaltic magmatism. However, previous studies of the Zhejiang Cenozoic basalts have focused on the Xinchang–Shengzhou flood basalts (Li et al., 2015; Liu et al., 2016b; Yu et al., 2017; Zou et al., 2000), which would have been readily affected by magma chamber processes (e.g., crustal contamination and fractional crystallization; Yu et al., 2015). Here, we present new major- and trace-element and Sr–Nd–Hf isotopic compositions of the Ninghai basalts, a new outcrop of Cenozoic basalts in eastern Zhejiang. More important, the Mg isotopic compositions, which are the good tracers for the recycling of carbonated components (e.g., Li et al., 2017; Teng, 2017; Wang et al., 2018; Yang et al., 2012), are also analyzed for the Ninghai basalts and those Xinchang–Shengzhou basalts without obviously crustal contamination. Based on these data, we argue that the high-SiO_2 basalts from Ninghai (detailed classification is shown in Section 4) were derived from a mantle source containing rutile-bearing eclogite, while nephelinite and basanite from both the Ninghai and Xinchang–Shengzhou were derived from a carbonated peridotite source. These two source components are attributed to the recycling of Pacific oceanic crust.

2. Geological background and sampling

Located at the eastern margin of Eurasia, Eastern China is composed of the Xing-Meng Block, North China Craton, Yangtze Craton, and Cathysia Block from north to south (Fig. 1a). The Precambrian Cathysia Block and Yangtze Craton converged to become the South China Block during the Proterozoic (Charvet et al., 1996). During the mid- to late-Mesozoic, the tectonics and volcanism of eastern China was controlled by the northwestward subduction of the paleo-Pacific oceanic crust, which also resulted in the development of northeast-trending faults in the South China Block (e.g., Chen and Jahn, 1998). These faults controlled the growth and evolution of Mesozoic basins where large volumes of basaltic magmas were erupted during the late Cenozoic, forming intraplate basalts (e.g., Ho et al., 2003; Zou et al., 2000).

Late Miocene basalts from Zhejiang represent the largest outcrop in southeast China, which are located at the east part of Zhejiang (Fig. 1a), near the northeastern boundary of the Cathysia Block. The outcrop includes the Xinchang–Shengzhou flood basaltic field and the Ninghai

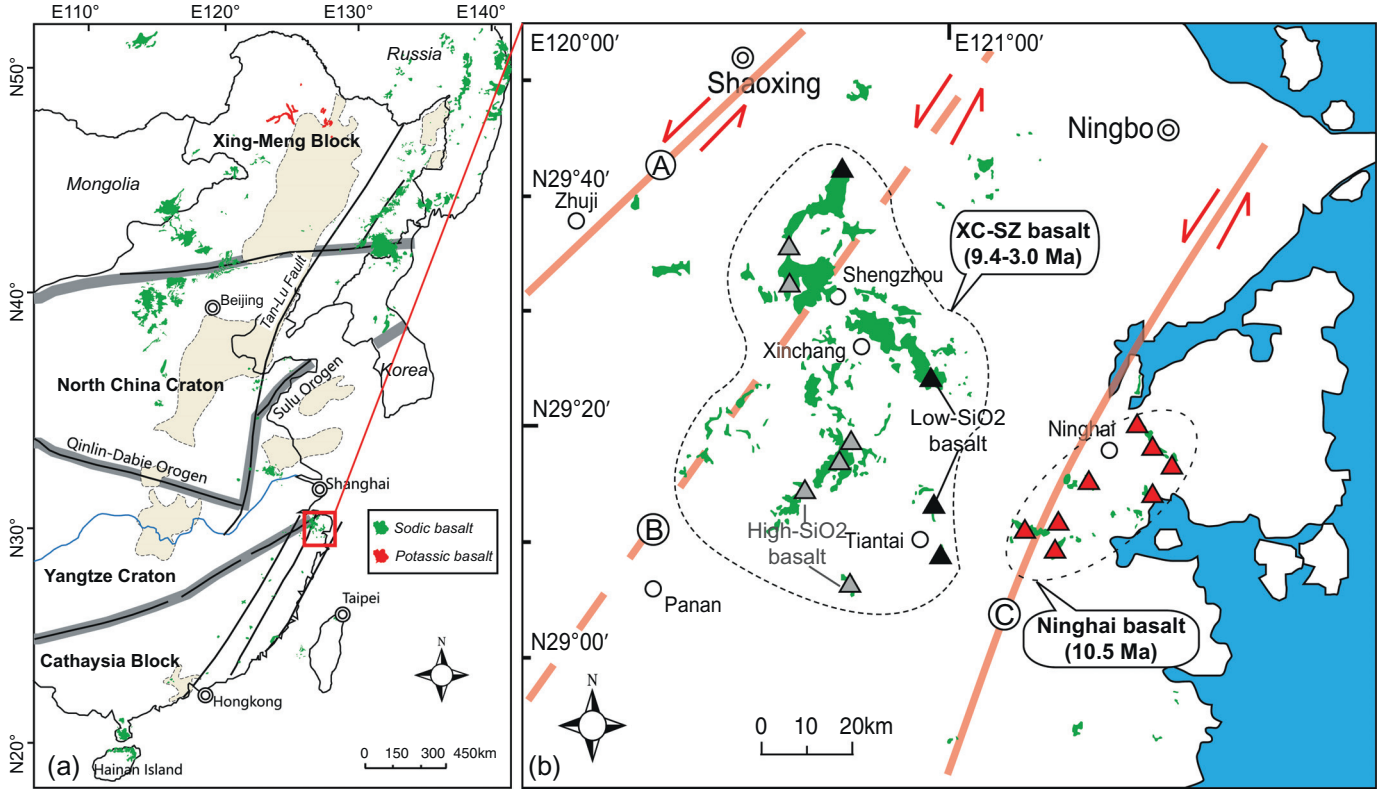

Fig. 1. Simplified geologic maps for Cenozoic basalts in eastern Asia (After Liu et al., 1992; Yarmolyuk et al., 2015) (a)and Zhejiang Province (b). Three major wrench faults in Zhejiang Province contain Jiangshan–Shaoxing fault (A), Lishui–Yuyao fault (B), and Zhenhai–Wenzhou fault (C). The sampling locations in Ninghai are shown as red triangles, and Xinchang–Shengzhou low-SiO_2 basalts are represented by black triangles, and Xinchang–Shengzhou high-SiO_2 basalts are represented by grey triangles in (b). Ages for basalts are after Ar-Ar dating work of Ho et al. (2003) and Yu et al. (2015). (For interpretation of the references to colour in this figure legend, the reader is referred to the web version of this article.)

basaltic field, which cover an area of about 600 km^2. The Xinchang–Shengzhou flood basaltic field was emplaced through more than five volcanic eruption episodes between 9.4 ± 0.1 Ma and 3.0 ± 0.1 Ma (Ho et al., 2003) along the Lishui–Yuyao Fault (Fig. 1b). The Ninghai basaltic field was emplaced through two eruption episodes with similar ages at 10.5 ± 0.5 Ma (Ho et al., 2003), and is cut by the Zhenhai–Ningyuan Fault (Fig. 1b). The lower eruption episodes of Xinchang–Shengzhou basalts are mainly composed of tholeiitic basalt, while the upper eruption episodes contain alkali olivine basalt and basanite. In comparison, basalts from the Ninghai basaltic field are mainly tholeiitic with minor basanite. We collected sixteen new basalt samples from Ninghai basaltic field for whole-rock geochemistry analyses, and the sampling locations of these samples almost cover the whole study area (See Fig. 1b). We also compiled published data on whole rock geochemistry in Zhejiang basalts (Li et al., 2015; Liu et al., 2016b; Yu et al., 2015, 2017; Zou et al., 2000) for comparison in this study. Due to the high vegetation coverage of study area, it is diffcult to identify the stratigraphic relationship for samples we collected from the Ninghai basaltic field.

In hand specimen, all Ninghai samples are massive to vesicular structure, and black to dark grey in colour. Most samples are fresh, but a few samples are slightly altered, in which olivine is partially to completely decomposed to iddingsite. These samples are either porphyritic (Supplementary Figure 1a) or aphyric (Supplementary Figure 1b) in texture. Basalts with porphyritic texture contain minor olivine phenocrysts (<10% modal abundance) set in a groundmass composed of plagioclase, olivine, clinopyroxene, Fe-Ti oxides and glass. Small amount of pyroxene phenocrysts are also observed. Furthermore, mantle xenoliths are common in the basalts from the Ninghai basaltic field.

3. Methods

Major and trace element compositions, as well as Sr, Nd, Hf isotopes were measured for all Ninghai samples. Mg isotopes were analyzed for

Table 1
Major and trace elemental compositions of Ninghai basalts.

No.	12NH03	12NH04	12NH05	12NH06	12NH07	12NH08	12NH09	12NH12	12NH13	12NH14	12NH15	12NH16	12NH17	12NH18	12NH19	12NH20
Major Element (wt%)																
SiO_2	48.91	50.43	50.96	51.74	50.59	48.54	49.27	44.57	44.61	44.7	49.03	49.41	49.86	47.96	50.29	49.78
TiO_2	2.251	2.527	2.585	2.276	2.488	2.744	2.721	2.882	2.928	2.911	3.312	2.969	3.038	2.439	3.067	3.046
Al_2O_3	12.5	12.51	12.89	13.2	13.47	12.45	12.51	11.53	11.53	11.54	12.82	12.59	12.77	12.19	12.89	12.98
$Fe_2O_3^T$[a]	11.71	12.65	12.12	11.96	11.71	12.58	12.58	13.73	13.75	13.93	13.29	12.78	12.99	12.66	12.28	11.85
MnO	0.141	0.169	0.157	0.148	0.142	0.146	0.164	0.186	0.176	0.182	0.1612	0.151	0.15	0.159	0.136	0.139
MgO	8.52	7.8	7.75	7.33	6.7	8.51	8.5	9.78	9.82	9.65	6.5307	8.04	8.07	9.47	6.82	5.79
CaO	9.14	9.22	9.35	9.18	9.24	9.45	9.41	10.44	10.4	10.25	9.02	9.18	9.26	9.9	9.06	9.5
Na_2O	2.55	2.36	2.56	2.62	2.65	2.40	2.47	2.75	2.83	3.10	2.95	2.77	2.71	2.63	2.63	2.73
K_2O	1.06	0.97	0.99	0.75	0.67	0.86	0.85	1.46	1.56	1.55	1.17	1.25	1.27	1.35	1.21	1.24
P_2O_5	0.358	0.376	0.371	0.273	0.301	0.414	0.42	0.842	0.871	0.859	0.4819	0.446	0.455	0.439	0.401	0.409
LOI	2.14	0.68	0	0.61	1.34	1.15	0.76	1.18	1.12	0.64	0.07	0	0	0.49	0.71	1.87
TOTAL	99.29	99.69	99.73	100.08	99.3	99.25	99.66	99.34	99.59	99.31	98.83	99.59	100.59	99.7	99.49	99.32
Trace Element (ppm)																
Li	11.4	3.83	5.60	7.16	7.89	6.22	6.13	7.75	8.53	7.94	5.96	8.13	8.38	6.91	9.35	10.5
Be	1.17	1.21	1.26	1.13	1.20	1.30	1.29	2.06	2.11	2.13	1.46	1.43	1.47	1.23	1.41	1.65
Sc	21.4	21.6	22.1	21.7	21.2	22.2	21.8	19.9	19.6	19.6	21.4	20.8	20.5	22.0	19.8	19.9
V	165	178	182	187	189	194	187	193	195	199	194	191	190	203	183	183
Cr	283	267	263	206	143	253	259	247	251	250	131	220	215	275	204	205
Co	47.3	53.4	49.2	47.4	45.1	53.5	51.9	60.4	56.2	58.1	49.9	51.8	51.3	54.6	47.8	47.0
Ni	206	236	193	164	126	231	220	254	252	254	121	175	170	203	171	162
Cu	69.5	68.1	68.2	64.1	62.9	73.6	71.1	115	125	117	66.0	63.6	64.2	75.4	54.0	57.9
Zn	107	124	129	114	114	125	123	135	135	136	136	131	131	116	129	126
Ga	18.9	20.1	20.6	20.0	20.6	21.3	21.0	21.6	21.4	21.8	22.8	22.0	21.9	19.9	21.9	22.3
Ge	1.23	1.41	1.43	1.43	1.36	1.40	1.37	1.33	1.41	1.41	1.43	1.42	1.38	1.38	1.40	1.36
Rb	20.2	20.8	21.0	18.0	13.6	19.6	16.3	34.5	33.5	35.2	22.9	26.3	26.1	34.5	25.6	25.8
Sr	488	506	503	419	467	567	558	940	984	925	579	627	623	556	590	638
Y	21.9	24.1	24.9	22.8	23.5	25.5	24.6	30.4	30.9	30.7	26.5	24.9	24.8	23.0	23.5	23.9
Zr	154	168	170	136	152	188	185	265	272	270	214	206	208	153	206	205
Nb	26.4	25.8	26.6	17.7	21.3	33.3	32.5	76.9	79.6	78.9	40.6	38.6	39.0	39.1	34.3	34.4
Cs	0.20	0.41	0.27	0.58	0.44	0.29	0.24	0.45	0.34	0.54	0.11	0.33	0.32	0.29	0.50	0.54
Ba	283	247	259	205	221	341	334	497	510	507	322	332	337	418	353	350
La	17.3	17.4	17.7	12.1	13.1	21.4	20.7	44.8	46.7	45.5	21.4	21.7	21.9	22.9	19.8	19.9
Ce	35.3	35.8	36.5	25.1	27.3	45.2	43.7	84.4	88.0	85.5	45.3	46.7	47.0	45.8	42.8	42.8
Pr	4.62	4.81	4.89	3.39	3.69	5.78	5.65	10.2	10.6	10.3	5.87	6.06	6.12	5.63	5.62	5.62
Nd	21.2	22.7	23.1	16.4	17.7	27.1	26.6	45.0	46.6	45.3	28.3	28.5	28.7	25.5	26.7	26.8
Sm	5.50	6.15	6.28	4.91	5.20	6.91	6.78	10.1	10.4	10.1	7.43	7.23	7.24	6.20	6.82	6.83
Eu	1.83	2.12	2.16	1.69	1.82	2.40	2.34	3.32	3.40	3.33	2.57	2.49	2.50	2.13	2.39	2.38
Gd	5.31	5.97	6.03	5.00	5.24	6.68	6.60	9.26	9.38	9.27	7.14	6.83	6.85	6.03	6.52	6.49
Tb	0.78	0.88	0.90	0.78	0.80	0.97	0.95	1.25	1.29	1.25	1.03	0.97	0.98	0.88	0.94	0.94
Dy	4.35	4.83	4.84	4.36	4.49	5.35	5.22	6.73	6.83	6.67	5.76	5.36	5.35	4.80	5.11	5.13
Ho	0.78	0.85	0.85	0.80	0.83	0.94	0.91	1.12	1.14	1.11	0.98	0.91	0.92	0.84	0.87	0.87
Er	1.91	2.07	2.12	1.99	2.04	2.34	2.23	2.70	2.75	2.68	2.39	2.23	2.25	2.10	2.14	2.12
Tm	0.25	0.27	0.27	0.27	0.27	0.29	0.28	0.33	0.33	0.33	0.30	0.28	0.28	0.27	0.26	0.27
Yb	1.51	1.58	1.56	1.57	1.58	1.72	1.61	1.81	1.82	1.80	1.68	1.58	1.55	1.53	1.49	1.49
Lu	0.20	0.21	0.21	0.22	0.22	0.23	0.22	0.24	0.24	0.24	0.23	0.21	0.21	0.21	0.20	0.20
Hf	3.57	3.95	3.96	3.30	3.65	4.47	4.36	5.77	5.90	5.71	5.01	4.79	4.80	3.59	4.85	4.80
Ta	1.43	1.43	1.47	0.98	1.18	1.85	1.80	4.01	4.20	4.06	2.26	2.10	2.12	2.00	1.93	1.91
Pb	1.89	2.09	1.96	1.89	1.63	2.31	2.18	3.20	3.29	3.20	1.45	2.01	2.01	2.14	2.26	2.19
Th	2.28	2.25	2.19	1.79	1.81	2.85	2.72	6.44	6.80	6.58	2.79	2.69	2.73	3.26	2.67	2.62
U	0.53	0.52	0.53	0.41	0.39	0.58	0.59	1.43	1.49	1.46	0.65	0.68	0.65	0.70	0.57	0.60

[a] $Fe_2O_3^T$, total iron as Fe_2O_3.

Table 2
Sr-Nd-Hf-Mg isotopic compositions of Ninghai and Xinchang-Shengzhou basalts.

No.	$^{87}Sr/^{86}Sr$	2SE[a]	$^{143}Nd/^{144}Nd$	2SE	ε_{Nd}[b]	$^{176}Hf/^{177}Hf$	2SE	ε_{Hf}[c]	$\delta^{25}Mg$ (‰)[d]	2SD[e]	$\delta^{26}Mg$ (‰)	2SSD	N
12NH03	0.704145	0.000009	0.512910	0.000010	5.31	0.282985	0.000003	7.53					
12NH04	0.703852	0.000007	0.512952	0.000009	6.13	0.283007	0.000003	8.31					
12NH05	0.703781	0.000007	0.512945	0.000012	5.99	0.283031	0.000003	9.16					
12NH06	0.703811	0.000007	0.512917	0.000015	5.44	0.283020	0.000005	8.77					
12NH07	0.703633	0.000006	0.512944	0.000013	5.97	0.283028	0.000003	9.05					
12NH08	0.703893	0.000009	0.512933	0.000010	5.76	0.282995	0.000004	7.89					
12NH09	0.703861	0.000006	0.512946	0.000010	6.01	0.283003	0.000003	8.17					
12NH12	0.703513	0.000009	0.512970	0.000004	6.48	0.283017	0.000003	8.66					
12NH13	0.703508	0.000007	0.512979	0.000006	6.65	0.283015	0.000003	8.59					
12NH14	0.703522	0.00001	0.512979	0.000005	6.65	0.283022	0.000003	8.84	−0.18	0.02	−0.36	0.02	4
12NH15	0.703361	0.00001	0.513001	0.000007	7.08	0.283046	0.000004	9.69					
12NH16	0.703768	0.000008	0.512968	0.000007	6.44	0.283029	0.000003	9.09	−0.14	0.04	−0.31	0.03	4
12NH17	0.703746	0.000009	0.512979	0.000012	6.65	0.283026	0.000003	8.98					
12NH18	0.703881	0.000007	0.512915	0.000008	5.40	0.283009	0.000003	8.38					
12NH19	0.703729	0.000009	0.512945	0.000010	5.99	0.283020	0.000003	8.77					
12NH20	0.703744	0.000006	0.512949	0.000012	6.07	0.283011	0.000003	8.45					
ZJ01*	0.703291	0.000007	0.512999	0.000002	7.04	0.283033	0.000002	9.23	−0.17	0.03	−0.35	0.06	4
ZJ02	0.703275	0.000008	0.512982	0.000003	6.71	0.283032	0.000003	9.19	−0.18	0.02	−0.36	0.06	4
ZJ03	0.703668	0.000006	0.512926	0.000002	5.62	0.283009	0.000006	8.37					
ZJ04	0.703904	0.000005	0.512932	0.000008	5.74	0.282998	0.000003	7.99	−0.17	0.02	−0.37	0.03	4
ZJ05	0.703936	0.000003	0.512928	0.000002	5.66	0.283006	0.000008	8.26					
ZJ06	0.703814	0.000004	0.512977	0.000003	6.61	0.283001	0.000004	8.10					
ZJ07	0.703843	0.000005	0.512954	0.000004	6.16	0.283011	0.000003	8.45	−0.19	0.01	−0.38	0.02	4
ZJ08	0.703826	0.000004	0.512963	0.000014	6.34	0.283001	0.000003	8.10					
ZJ09	0.703869	0.000005	0.512929	0.000003	5.68	0.283014	0.000009	8.57					
ZJ10	0.704345	0.000005	0.512922	0.000003	5.54	0.282990	0.000003	7.71					
ZJ11	0.704237	0.000005	0.512926	0.000003	5.62	0.282995	0.000005	7.89					
ZJ12	0.703765	0.000003	0.512926	0.000002	5.62	0.283008	0.000006	8.34	−0.15	0.03	−0.32	0.05	4
ZJ13	0.703801	0.000006	0.512939	0.000005	5.87	0.283005	0.000004	8.24					
ZJ14	0.703786	0.000010	0.512905	0.000003	5.21	0.283012	0.000007	8.49					
ZJ15	0.703952	0.000006	0.512855	0.000011	4.23	0.282996	0.000003	7.92					
ZJ16	0.703862	0.000005	0.512825	0.000004	3.65	0.283011	0.000007	8.46					
ZJ17	0.704070	0.000007	0.512878	0.000004	4.68	0.282985	0.000003	7.53	−0.15	0.01	−0.29	0.02	4
ZJ18	0.703925	0.000005	0.512819	0.000004	3.53	0.282999	0.000006	8.02	−0.15	0.03	−0.31	0.04	4
ZJ19	0.703591	0.000004	0.512884	0.000003	4.80	0.283029	0.000005	9.08					
ZJ20	0.703764	0.000007	0.512866	0.000004	4.45	0.282970	0.000006	7.02					
ZJ21	0.703769	0.000009	0.512869	0.000004	4.51	0.282973	0.000007	7.12	−0.16	0.04	−0.30	0.05	4
ZJ22	0.704240	0.000005	0.512858	0.000003	4.29	0.282950	0.000007	6.30					
ZJ23	0.703756	0.000005	0.512904	0.000002	5.19	0.282965	0.000006	6.81					
ZJ24	0.703797	0.000006	0.512916	0.000009	5.42	0.282966	0.000002	6.86					
ZJ25	0.704275	0.000004	0.512858	0.000003	4.29	0.282950	0.000008	6.31					
ZJ26	0.704335	0.000008	0.512844	0.000005	4.02	0.282946	0.000002	6.15					

[a] SE refers to standard error.
[b] $\varepsilon_{Nd} = [(^{143}Nd/^{144}Nd)_{sample}/(^{143}Nd/^{144}Nd)_{CHUR}-1]*10^4$; where $(^{143}Nd/^{144}Nd)_{CHUR} = 0.512638$.
[c] $\varepsilon_{Hf} = [(^{176}Hf/^{177}Hf)_{sample}/(^{176}Hf/^{177}Hf)_{CHUR}-1]*10^4$; where $(^{176}Hf/^{177}Hf)_{CHUR} = 0.282772$.
[d] $\delta^{x}Mg = \{(^{x}Mg/^{24}Mg)_{sample}/(^{x}Mg/^{24}Mg)_{DSM3}-1\} \times 1000$, where X = 25 or 26 and DSM3 is a Mg standard solution made from pure Mg metal (Galy et al., 2003).
[e] 2SD = twice the standard deviation of the population of N($N \geq 4$) repeat measurements of a sample solution.
* , Sr, Nd, and Hf isotopic compositions of ZJ-X (X = 1–26) samples are from Yu et al. (2017).

those selected fresh Ninghai and Xinchang–Shengzhou basalts with less crustal contamination. For example, nephelinites and basanites from low-SiO_2 basalts and high-SiO_2 basalts formed by magmatic recharge, which means continuous or episodic magma replenishment in the long-lived magma chambers above a region undergoing relatively continuous magmatic fluxing (Yu et al., 2017). New chemical and isotopic data for Ninghai basalts are listed in Table 1 and Table 2, whereas those for international standards and reduplicated samples are given in Supplementary Table 1, Supplementary Table 2, and Supplementary Table 3. The published data for Xinchang–Shengzhou basalts are from Yu et al. (2015, 2017).

Samples were first crushed into gravel-size chips. Clean chips were then pulverized in a corundum mill. The measurements of whole-rock major and trace elements were carried out at the Department of Geology, Northwest University in Xi'an, China. Major elements were determined by a Rix-2100X-ray fluorescence spectrometer (XRF). The results of diverse standards (BHVO-2, BCR-2, and GSR-3) suggest the uncertainties are less than ±1% for elements Si, Ti, Al, Fe, Mn, Mg, Ca, K, and P, and about ±5% for Na (Supplementary Table 1). Trace elements, including the rare earth elements (REEs), were measured with an ELANG100DRC inductively coupled plasma mass spectrometer (ICP-MS) after the acid digestion conducted in Teflon bombs. Analyses of the USGS rock standards (BHVO-2, AGV-2, BCR-2 and GSP-1; reference data are from Jochum et al. (2016)) indicate the precision and accuracy are better than 5% for Sc, V, Co, Ni, Rb, Sr, Y, Zr, Nb, Ba, Ta, Th, U and REEs, and 10% for Cr, Cs, Hf, and Pb (STable 2). Isotopic analyses of Sr, Nd and Hf were performed at the State Key Laboratory for Mineral Deposits Research, School of Earth Sciences and Engineering at Nanjing University. Mg isotopic analyses were performed at the Institute of Geology and Geophysics, Chinese Academy of Sciences, Beijing. All chemical digestion and separation were carried out in Class 100 ultra-clean laboratory and the mass spectrometric analyses were performed in Class 1000 clean laboratories. Reagents used for leaching, dissolution and separation were twice-distilledextra-pure grade, dilutions were made using ≥18.2 MΩ cm^{-1}de-ionized water, and all labware was acid-washed prior to use.

Isotopic ratios of Sr and Nd were measured on a TRITON Tl (Thermo Finnigan) thermal ionization mass spectrometer (TIMS) in static mode with relay matrix rotation on single W (Sr) or double Re (Nd) filaments. 100 mg sample powders were leached for 12 h in warm 2.5 N HCl, and dissolved in a hot HF-HNO_3 mixture followed by ion exchange procedures. Detailed analytical procedures for Sr and Nd isotopes are given

by Yu et al. (2017). Sr and Nd isotopic compositions were normalized to $^{86}Sr/^{88}Sr = 0.1194$ and $^{146}Nd/^{144}Nd = 0.7219$. During the analytical session for our samples, the measured values for the NBS987 Sr standard and JNdi-1 Nd standard were 0.710239 ± 0.000002 for $^{87}Sr/^{86}Sr$ and 0.512128 ± 0.000004 for $^{143}Nd/^{144}Nd$, respectively. Measured $^{87}Sr/^{86}Sr$ and $^{143}Nd/^{144}Nd$ values for BCR-2 were 0.705018 ± 0.000003 and 0.512624 ± 0.000004 (Reference values are 0.705019 ± 0.000016 and 0.512634 ± 0.000012 from Weis et al. (2006)). The total procedure blanks for Sr and Nd isotopes were <100 pg and 60 pg.

Hf isotopic data were obtained using a Neptune plus (Thermo Fisher Scientific) multi-collector inductively coupled plasma mass spectrometer (MC-ICP-MS). 100 mg powders were leached for 12 h in warm 2.5 N HCl, and dissolved in 15 ml Teflon beakers in an HF-$HClO_4$ acid mixture at 120 °C for >5 days. After evaporation to dryness, all samples were dried at 200 °C in order to break CaF bonds. Finally, the samples were dissolved in 3 N HCl. Hafnium was separated from the rock matrix by ion exchange procedures using Eichrom® Ln-Spec resin. The detailed analytical procedure for the Hf isotopic measurement can be found in Yang et al. (2010). Hf isotopic ratios were normalized to $^{179}Hf/^{177}Hf = 0.7325$. Repeated measurements of the JMC 475 Hf standard gave a mean $^{176}Hf/^{177}Hf$ value of 0.282157 ± 0.000005. Reported results were then normalized to the $^{176}Hf/^{177}Hf$ value of 0.282160 (Vervoort et al., 1999) using the daily average of the JMC 475 Hf standard. Measured values for BHVO-2 and BCR-2 were 0.283082 ± 0.000004 and 0.282857 ± 0.000006 (Reference values are 0.283101 ± 0.000026 and 0.282867 ± 0.000018 from Weis et al. (2007)). The total procedure blank for Hf isotope was <50 pg.

Mg isotopic data were obtained using a Neptune (Thermo Fisher Scientific) multi-collector inductively coupled plasma mass spectrometer (MC-ICP-MS) following the procedures described in detail by An et al. (2014). Approximately 20 mg and 50 mg of sample powders and USGS reference materials (BCR-2, BHVO-2, BIR-1 and GSP-2) were weighed and fully dissolved in a mixture of concentrated HF-HNO_3. The clear solutions with 20 μg Mg were then dried and dissolved in 2 N HNO_3 for column chemical analysis. Detailed procedures of Mg purification can refer to An et al. (2014). During the purification, we also prepared a synthetic multi-element standard solution IGGMg1-A (K:Al:Fe:Na:Ca:Mg:Mn:Rb:Ti:Zn:Cs:Cu = 20:10:8:5:5:1:1:0.2:0.1:0.02:0.01:0.01) to examine the purification efficiency of the column. The Mg yields of all standards and unknown samples were better than 99.7%, and the total Mg blank was <6 ng. Mg isotopic compositions were measured by the sample-standard bracketing method in a medium resolution mode. The signal intensity for ^{24}Mg was generally about 4–5 V/ppm and the average blank were <2 mV. Each sample was measured at least 4 times and then averaged. Mg isotopic data are expressed in δ notation as per mil (‰) deviation from DSM3 (Galy et al., 2003). The long-term external precision determined by repeated analyses of the international Mg standards (DSM3 and Cambridge1), in-house Mg standards (IGGMg1, IGGMg2, and SRM980, (An et al., 2014)) is better than 0.06‰ (2SD) for $\delta^{26}Mg$, where IGGMg1 and IGGMg2 are mono-elementalICP-MS Mg standards (1000 ppm in 1 N HNO_3) made by the National Center of Analysis and Testing for Nonferrous Metals and Electronic Materials. Repeated measurements of the Cambridge1 and in-house Mg standard IGGMg1at different dates yielded average $\delta^{26}Mg$ values of −2.60‰ ± 0.04‰ (2SD, $n = 26$) and − 1.76‰ ± 0.04‰ (2SD, $n = 70$), respectively.

4. Geochemical results

The Ninghai basalt samples are characterized by moderate to high SiO_2, and variable MgO, $Fe_2O_3^T$, and TiO_2 contents (Table 1). For comparison, the Xinchang–Shengzhou flood basalts are shown which were divided into low-SiO_2 (SiO_2 < 47.5 wt%) and high-SiO_2 (SiO_2 > 47.5 wt%) groups (Yu et al., 2015, 2017). The Xinchang–Shengzhoulow-SiO_2 basalts have low SiO_2 (39.1–47.4 wt%), and high MgO (8.58–11.4 wt%), $Fe_2O_3^T$ (13.1–16.2 wt%), and TiO_2 (2.16–3.58 wt%) contents. The Xinchang–Shengzhouhigh-SiO_2 basalts have high SiO_2 (48.1–52.6 wt%), and low MgO (5.18–7.89 wt%), $Fe_2O_3^T$ (11.5–12.5 wt%), and TiO_2 (2.0–3.0 wt%) contents (Yu et al., 2015, 2017). According to the classification of Le Bas et al. (1986), the Ninghai basalt samples include basanites and basalts, whereas the Xinchang–Shengzhou basalt samples include nephelinites, basanites, basalts, trachybasalts, and basaltic andesites (Fig. 2a). MgO is positively correlated with CaO/Al_2O_3(Fig. 2b) and Ni (Fig. 2d) in the Ninghai and Xinchang–Shengzhou samples. No correlation is observed between MgO and Sc in the Ninghai samples (Fig. 2c). For convenience, the Ninghai basalts are also classified into low-SiO_2 (basanite) and high-SiO_2 (basalt) groups according to their SiO_2 contents (Fig. 1).

In the primitive-mantle-normalizedmulti-element diagram (Fig. 3), all samples are characterized by enrichment in highly incompatible elements, and positive Nb, Ta, and negative Pb anomalies, similar to ocean island basalt (OIB; Hofmann et al., 1986). The degree of enrichment decreases from nephelinites to basaltic andesites (Fig. 3). The Ninghai low-SiO_2 basalts exhibit negative Hf ($Hf/Hf^* = 0.67–0.68$; $Hf/Hf^* = Hf_N/(Sm_N \times Nd_N)^{0.5}$, where N indicates normalized to primitive mantle) and Ti ($Ti/Ti^* = 0.77–0.78$; $Ti/Ti^* = Ti_N/(Nd_N^{-0.055} \times Sm_N^{0.333} \times Gd_N^{0.722})$) anomalies, similar to the Xinchang–Shengzhoulow-SiO_2 basalts ($Hf/Hf^* = 0.58–0.76$, $Ti/Ti^* = 0.80–0.97$), while other samples yield values of Hf/Hf^* and Ti/Ti^* values of 0.72–0.96 and 1.02–1.20, respectively. In chondrite-normalizedREE patterns, there are no Eu anomalies (Supplementary Figure 2). In addition, all basalt samples have variable Ce/Pb and Nb/U ratios, with ranges larger than those of MORB and OIB(Hofmann et al., 1986).

Sr–Nd–Hf isotopic compositions have limited ranges (Table 2), but are well correlated with each other. Compared with Cenozoic basalts from eastern China, samples of the present study are relatively depleted. The Sr–Nd–Hf isotopic compositions of the Ninghai and Xinchang–Shengzhou samples indicate the mixing of two end-members, where ε_{Nd} correlates negatively with $^{87}Sr/^{86}Sr$ and positively with ε_{Hf}(Fig. 4a, b). In plot of ε_{Nd} versus ε_{Hf}, both Ninghai samples and Xinchang–Shengzhoulow-SiO_2 basalts are located below the mantle array (Fig. 4b), similar to Pacific Ocean MORB. To evaluate the degree of Nd-Hf decoupling, we calculated $\Delta\varepsilon_{Hf}$ values, where $\Delta\varepsilon_{Hf}$ is the difference in ε_{Hf} relative to the ε_{Nd}–ε_{Hf} mantle array, defined as $\Delta\varepsilon_{Hf} = \varepsilon_{Hf} - 1.55\varepsilon_{Nd} - 1.21$ (Vervoort et al., 2011). The Ninghai and Xinchang–Shengzhou samples yield $\Delta\varepsilon_{Hf}$ values of −3.7 to +1.4, which are well correlated with Sr and Nd isotopic compositions. For Mg isotopic compositions, the Ninghai and Xinchang–Shengzhou samples, as well as the international standards (Supplementary Table 3), fall along the mass-dependent fractionation line for Mg isotopes (Supplementary Figure3; Young and Galy 2004). All samples have $\delta^{26}Mg$ values ranging from −0.29‰ to −0.38‰ (Fig. 4c, d), lower than those of terrestrial mantle ($\delta^{26}Mg = -0.23‰ \pm 0.04‰$, Lai et al., 2015; $\delta^{26}Mg = -0.25‰ \pm 0.04‰$, Teng 2017). In addition, $\delta^{26}Mg$ shows weak positive correlations with $^{87}Sr/^{86}Sr$ (Fig. 4c) and $\Delta\varepsilon_{Hf}$, and negative correlations with ε_{Nd}(Fig. 4d) and ε_{Hf}.

5. Discussion

5.1. Weathering processes, fractional crystallization, and crustal contamination

Geochemical differences between intraplate basalts can be produced by shallow processes such as surface weathering and magma chamber processes (e.g., Carlson et al., 1981; Kumar et al., 2010), in addition to source heterogeneity (e.g., Chen et al., 2009; Liu et al., 2016b; Xu, 2014; Zou et al., 2000). These shallow processes should be evaluated prior to a discussion of basalt origin. The relatively low LOI values (<2 wt%) and the fresh appearance of hand specimens indicate that weathering has little influence on the geochemical compositions of the investigated basalts. This is also verified by the good correlations

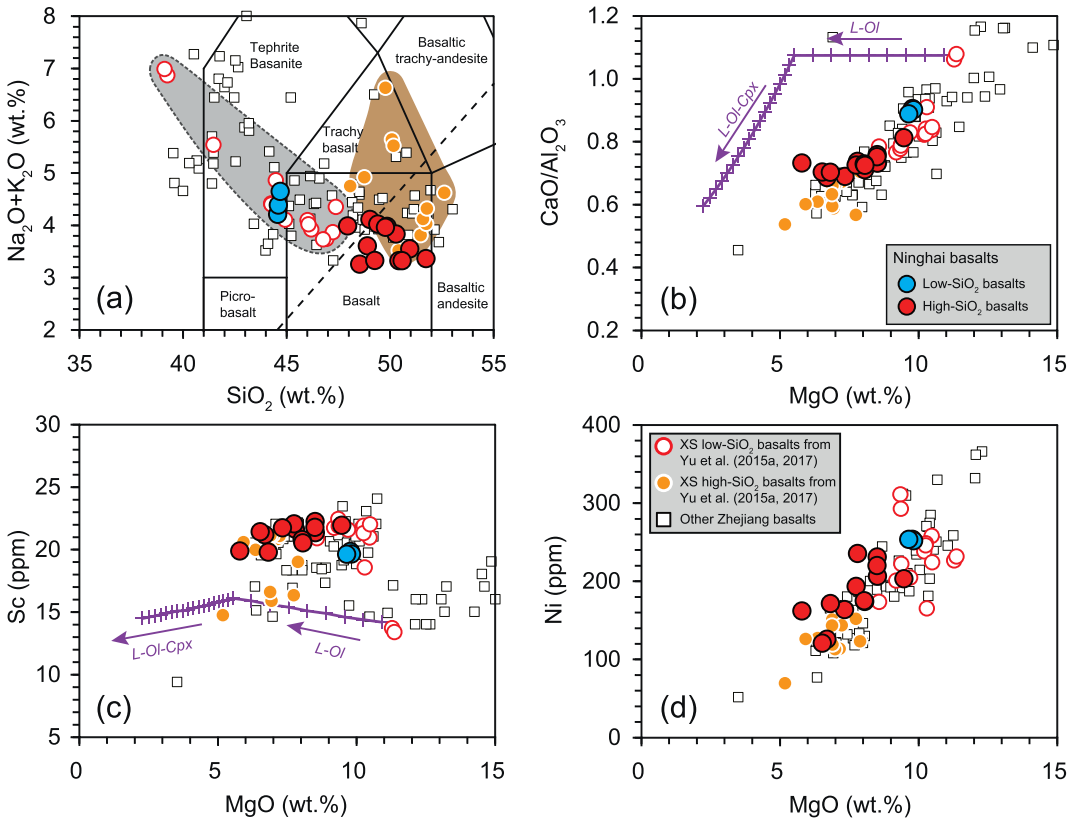

Fig. 2. Variations of SiO_2 versus total alkali (a), and MgO versus CaO/Al_2O_3, Sc, and Ni (b-d) for Ninghai, Xinchang–Shengzhou basalts and basalts from other places of Zhejiang. Data for published Cenozoic basalts from Zhejiang(Ho et al., 2003; Li et al., 2015; Liu et al., 2016b; Zou et al., 2000) are presented as comparison. In (b)and (c), we used Petrolog 3 software (Danyushevsky and Plechov, 2011) to model the compositional variation of CaO/Al_2O_3 and Sc as a function of olivine and clinopyroxene removal from Zhejiang basalts.

between Nb and other strongly incompatible elements such as Sr, La, and U (Supplementary Figure 4).

Radiogenic isotopic data from previous studies indicate that some of the Xinchang–Shengzhou basalts were affected by crustal contamination (Yu et al., 2015, 2017). To evaluate the role of crustal contamination, Nb/U and Ce/Pb ratios were examined in this study (Fig. 5a), because continental crust is characterized by lower Nb/U and Ce/Pb ratios (Nb/U_{LCC} = 25, Nb/U_{UCC} = 4; Ce/Pb_{LCC} = 5, Ce/Pb_{UCC} = 3.7; Rudnick and Gao, 2014) than DMM (Nb/U = 46.4, Ce/Pb = 30.6; Workman and Hart, 2005). Therefore, low Nb/U and Ce/Pb ratios for those Xinchang–Shengzhouhigh-SiO_2 basalts and low-volume Ninghai high-SiO_2 basalts (Fig. 5a) indicate the significant influence of crustal contamination. In comparison, most Ninghai basalts and Xinchang–Shengzhoulow-SiO_2 basalts show OIB-like Nb/U and Ce/Pb ratios,

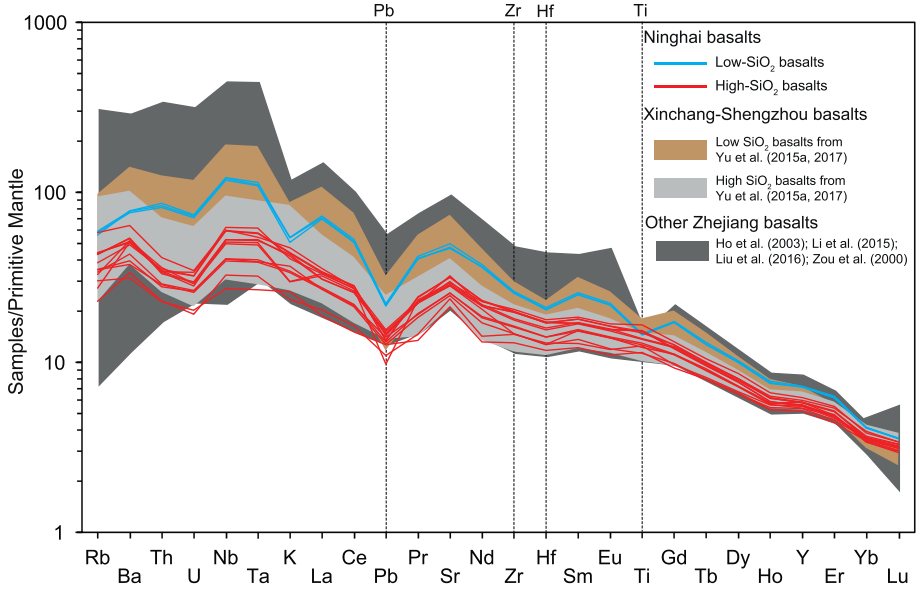

Fig. 3. Whole rock trace element abundances for Ninghai and Xinchang–Shengzhou basalts and basalts from other places of Zhejiang. The primitive mantle values are from McDonough and Sun, (1995).

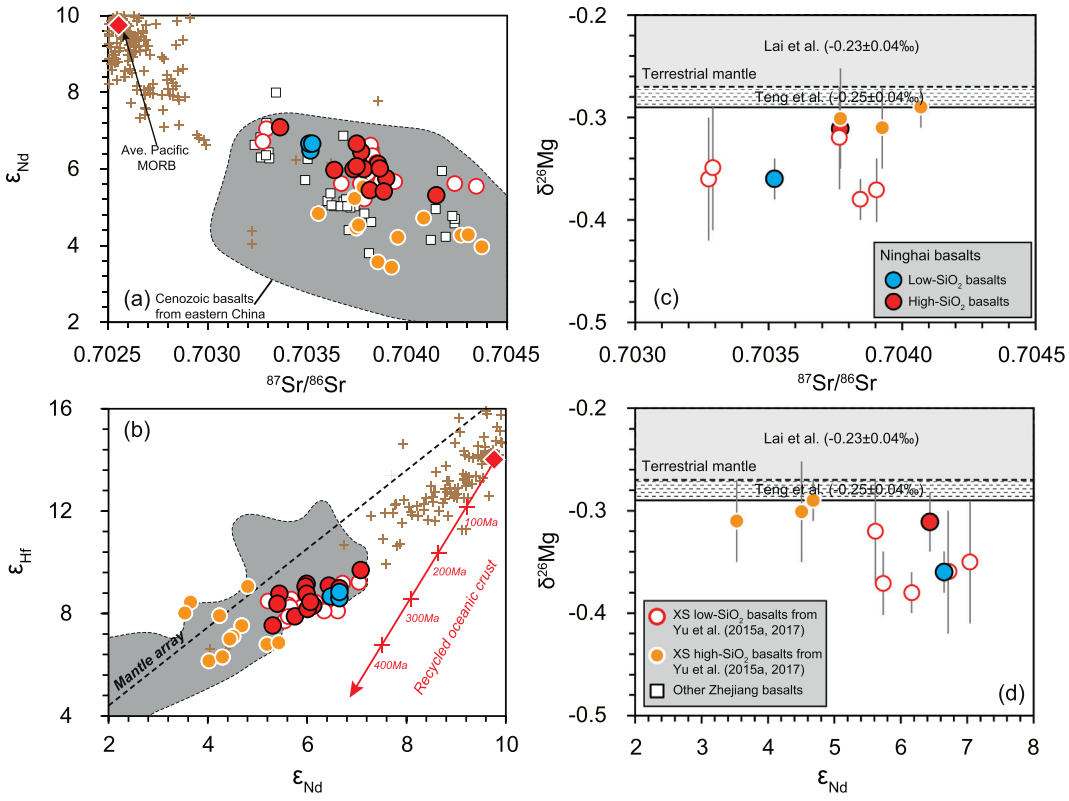

Fig. 4. $^{87}Sr/^{86}Sr$, and ε_{Hf} versus ε_{Nd} (a, b)and $^{87}Sr/^{86}Sr$, ε_{Nd} versus $\delta^{26}Mg$ (c, d)for Ninghai and Xinchang–Shengzhou basalts. The mantle array line in (b)is from Vervoort et al. (2011). The isotopic data of Pacific Ocean MORB in (a)and (b)are from Petrological Database (http://www.earthchem.org/petdb). For comparison, published data for some Cenozoic basalts from eastern China (Chen et al., 2009; Chen et al., 2016; Guo et al., 2016; Li et al., 2015; Li et al., 2017; Sakuyama et al., 2013; Wang et al., 2011; Xu, 2014; Xu et al., 2012; Xu et al., 2017; Zhang et al., 2009; Zhang and Guo, 2016; Zou et al., 2000) are shown in (a) and (b). The horizontal grey bar ($\delta^{26}Mg = -0.23 \pm 0.04$‰) and striped bar ($\delta^{26}Mg = -0.25 \pm 0.04$‰) stand for recommended $\delta^{26}Mg$ values of the terrestrial mantle, and the data are from Lai et al. (2015) and Teng, (2017). In Figure(b), the Nd-Hf isotopic compositions of recycled Pacific oceanic crust at various times are shown as evolutionary path (red line), which was calculated by using average present-day isotopic composition of Pacific MORB from Petrological Database (http://www.earthchem.org/petdb). Error bars represent 2SD (2 times the standard deviation) uncertainties. (For interpretation of the references to colour in this figure legend, the reader is referred to the web version of this article.)

indicating negligible influence of crustal contamination, consistent with the conclusions of previous studies (Li et al., 2015; Liu et al., 2016b; Yu et al., 2015, 2017). The negative correlation between MgO and ε_{Hf} for the Ninghai basalts (Fig. 5b) also supports this proposal. In contrast, the Xinchang–Shengzhouhigh-SiO_2 basalts show a positive correlation between MgO content and ε_{Hf} (Fig. 5b), again indicating the potential influence of crustal contamination as continental crust is characterized by low MgO contents and enriched Hf isotopic compositions (Rudnick and Gao, 2014). We argue that crustal contamination was insignificant for most of the Ninghai basalts and Xinchang–Shengzhoulow-SiO_2 basalts.

Petrographic characteristics and whole-rock compositions record fractional crystallization. The presence of olivine phenocrysts in some Ninghai basalts indicates the role of olivine fractionation in the basaltic melts, which is also suggested by the positive correlation between MgO and Ni contents (Fig. 2d). For Ninghai samples and Xinchang–Shengzhoulow-SiO_2 basalts, though they show a positive correlation between MgO and CaO/Al_2O_3 (Fig. 2b), no correlation is observed between MgO and Sc contents (Fig. 2c). This indicates that fractional

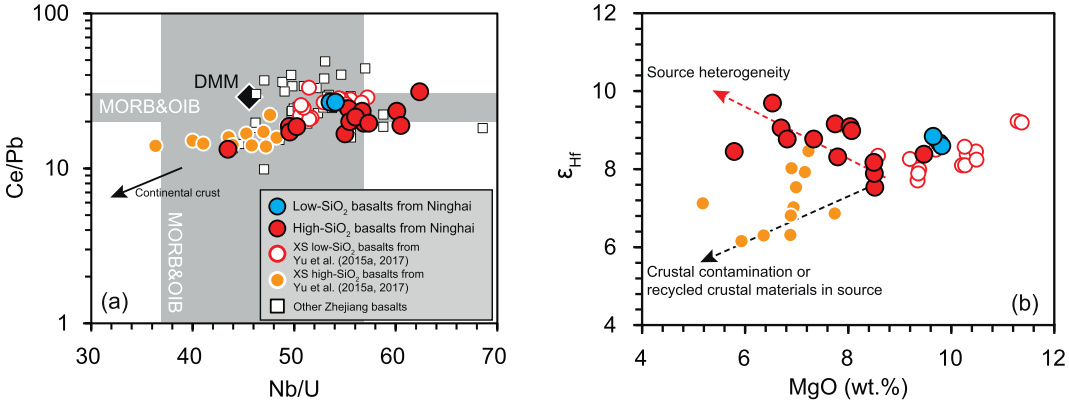

Fig. 5. Nb/U versus Ce/Pb (a)and MgO versus ε_{Hf} (b)for Ninghai and Xinchang–Shengzhou basalts. Data for published Cenozoic basalts from Zhejiang(Ho et al., 2003; Li et al., 2015; Liu et al., 2016b; Zou et al., 2000) are presented as comparison. Data for DMM (depleted MORB mantle) is from Workman and Hart, (2005). The shadow stands for the area of data of MORB and OIB (Hofmann et al., 1986).

crystallization of clinopyroxene had little influence on the observed geochemical variations. In contrast, the Xinchang–Shengzhouhigh-SiO_2 basalts exhibit positive correlations between MgO and CaO/Al_2O_3, and between MgO and Sc, indicating clinopyroxene fractionation. Petrolog 3 software (Danyushevsky and Plechov, 2011) was used to model CaO/Al_2O_3 (Fig. 2b) and Sc (Fig. 2c) variations as a function of olivine and clinopyroxene removal for the Ninghai and Xinchang–Shengzhou basalts. For modeling, we selected the nephelinite samples with compositions approaching the primary magma composition. With decreasing of CaO/Al_2O_3 ratios, the Ninghai samples and Xinchang–Shengzhoulow-SiO_2 basalts show higher MgO and Sc contents than the modeling results (Fig. 2b), indicating that the basalts underwent solely olivine fractionation. However, for the Xinchang–Shengzhouhigh-SiO_2 basalts, the modeling curves of clinopyroxene fractionation are consistent with the evolutionary trends. At lower MgO contents, the Zhejiang basalts show relatively constant, or slightly increased, TiO_2 contents (Supplementary Figure 5), indicating negligible fractionation of Fe-Ti oxides and other Ti-bearing minerals.

To exclude the potential effects of crustal contamination and fractionation of clinopyroxene, Fe-Ti oxides, and other Ti-bearing minerals, the geochemical compositions of basalts with MgO > 6 wt% and Nb/U > 45 (Fig. 5a) from Ninghai, Xinchang–Shengzhou, and other parts of Zhejiang were selected for discussion of their mantle source characteristics or partial melting processes in the following sections. In addition, data of the Xinchang–Shengzhouhigh-SiO_2 basalts, which formed by magmatic recharge (with minor crustal contamination), are also plotted in Figs. 6, 7, and 8(Yu et al., 2015, 2017).

5.2. Source lithologies of the Ninghai and Xinchang–Shengzhou basalts

Variations in elemental ratios can be controlled by both partial melting and source heterogeneity. The La/Yb and Sm/Yb ratios of basalts can be used to indicate the degree of partial melting (Supplementary Figure 6), as heavy rare earth elements (HREEs) are compatible in garnet (e.g., Johnson, 1998). The Ninghai high-SiO_2 basalts have lower La/Yb and Sm/Yb ratios than those of low-SiO_2 basalts from Xinchang–Shengzhou and Ninghai, indicating a higher degree of melting for the high-SiO_2 samples (Supplementary Figure6). However, variable degrees of partial melting of the same source would not affect the Sr–Nd–Hf isotopic compositions of basalts. Therefore, good correlations between the Sr–Nd–Hf–Mg isotopic compositions (Fig. 4) of low-SiO_2 basalts from Xinchang–Shengzhou (mainly nephelinites and basanites) and Ninghai, and between their Ti/Ti* and isotopic compositions (Fig. 6a, b), cannot be explained by differences in the degree of partial melting alone, thus indicating that source heterogeneity played an important role in the formation of these basalts.

As all the basalts have OIB-liketrace-element signatures (Fig. 3), there are several possible source lithologies: (1)fertile peridotite/hornblendite/secondary pyroxenite that was previously metasomatized by slab-derived fluids/melts (e.g., Pilet et al., 2008; Sobolev et al., 2005; Yaxley, 2000), (2)eclogite/pyroxenite derived from slab or directly from sediments (e.g., Hirschmann et al., 2003; Irifune et al., 1994; Kogiso et al., 2003), and (3)carbonated peridotite/eclogite derived from the recycling of carbonated components (e.g., Dasgupta et al., 2007; Gerbode and Dasgupta, 2010). These potential source components are considered in the following sections.

5.2.1. Asthenospheric mantle contaminated by recycled sediments

The correlations observed between the Sr–Nd–Hf isotopic compositions of the Ninghai basalts and the Xinchang–Shengzhoulow-SiO_2 basalts indicate the mixing of two end-members in the source (Fig. 4a, b). One end-member is characterized by moderate radiogenic isotopes (more enriched than those of Pacific MORB) (Fig. 4a, b). However, this end-member shows a weak Ti anomaly, similar to DMM (Fig. 6)

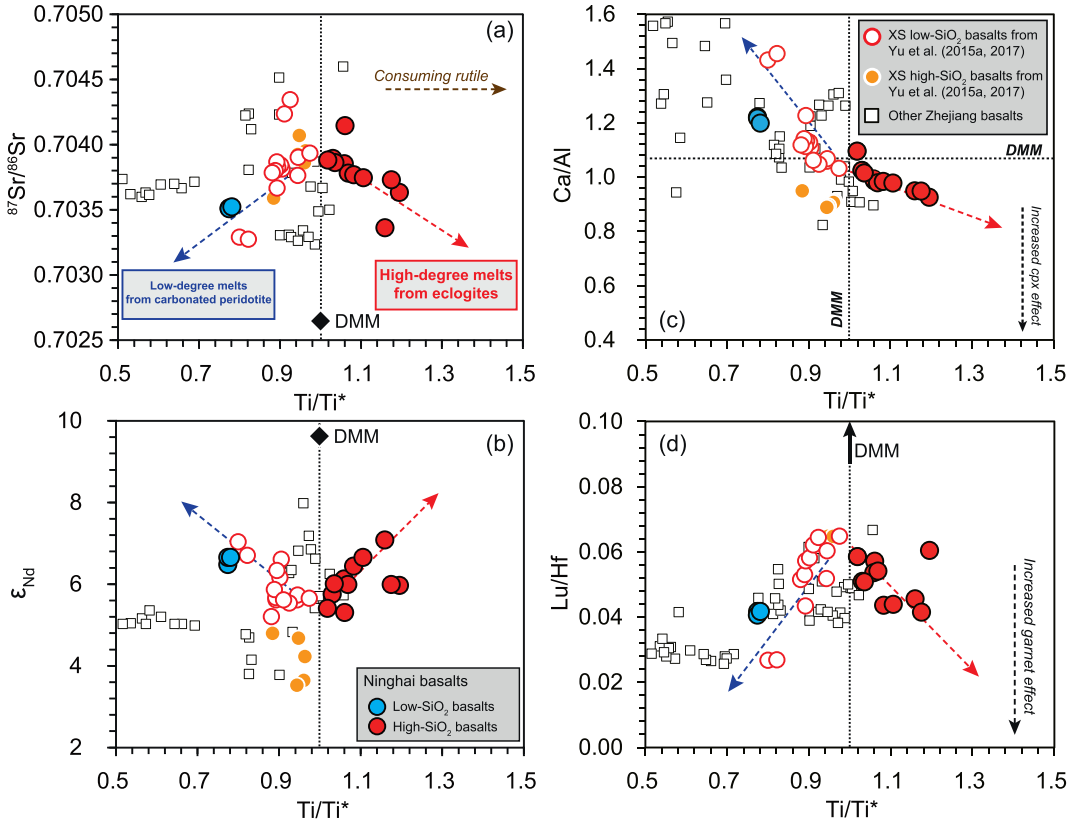

Fig. 6. Variations in Ti/Ti* versus $^{87}Sr/^{86}Sr$ (a), ε_{Nd} (b), Ca/Al (c), and Lu/Hf (d)for Ninghai and Xinchang–Shengzhou basalts and basalts from other places of Zhejiang. Data for published Cenozoic basalts from Zhejiang(Ho et al., 2003; Li et al., 2015; Liu et al., 2016b; Zou et al., 2000) are presented as comparison. Data for DMM (depleted MORB mantle) is derived from Workman and Hart, (2005). Only samples with little influence from crustal contamination (Nb/U > 45) and fractional crystallization (MgO > 6 wt%) are picked up for comparison.

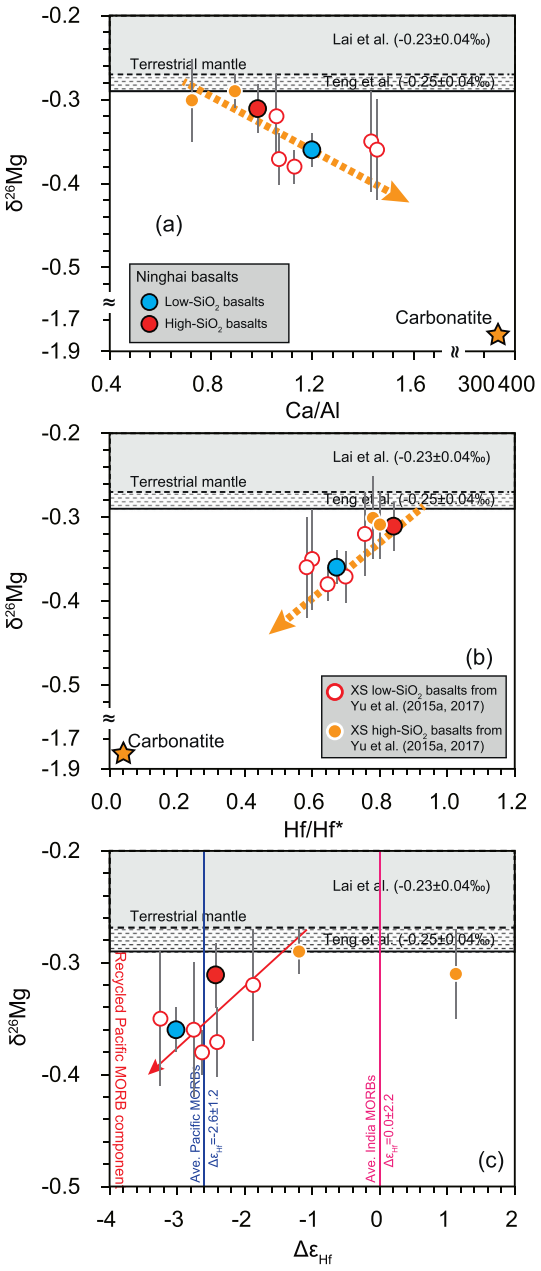

Fig. 7. Plots of δ^{26}Mg versus Ca/Al (a), Hf/Hf* (b)and $\Delta\varepsilon_{Hf}$ (c)for Ninghai and Xinchang–Shengzhou basalts. The horizontal grey bar ($\delta^{26}Mg = -0.23 \pm 0.04$‰) and striped bar ($\delta^{26}Mg = -0.25 \pm 0.04$‰) stand for recommended δ^{26}Mg values of the terrestrial mantle, and the data are from Lai et al. (2015) and Teng, (2017). The average elemental data for continental and oceanic carbonatites are from Hoernle et al. (2002). The Mg isotopic composition of carbonatites can be referred to Li et al. (2017) and references therein. Average $\Delta\varepsilon_{Hf}$ values in (c)of Indian Ocean MORB and Pacific Ocean MORB are calculated from Petrological Database (http://www.earthchem.org/petdb). Only samples with little influence from crustal contamination (Nb/U > 45) and fractional crystallization (MgO > 6 wt%) are picked up for comparison. Error bars represent 2SD (2 times the standard deviation) uncertainties.

(Workman and Hart, 2005). The OIB-like trace elemental patterns of these basalts (Fig. 3) indicate their derivation from the asthenospheric mantle (Li et al., 2015; Liu et al., 2016b; Yu et al., 2015, 2017). Recent studies of OIB in the western Pacific have observed similar isotopic characteristics, which are also considered the result of melting of the asthenospheric mantle (e.g., Jackson et al., 2017). The moderate radiogenic isotopes of this end-member are explained by contributions from recycled sediments (Liu et al., 2016b), and this signature is particularly pronounced in the Xinchang–Shengzhouhigh-SiO_2 basalts (Yu et al., 2017). Mg isotopic compositions of this end-member are close to that of the terrestrial mantle (Fig. 4c, d), indicating that carbonate is free in these recycled sediments. In this study, we pay more attention to the other end-member, which is characterized by depleted radiogenic isotopes and light Mg isotopic compositions (Fig. 4).

5.2.2. Carbonated peridotite source

The Ninghai low-SiO_2 basalts are characterized by negative Zr, Hf, and Ti anomalies (Ti/Ti* = 0.77–0.78; Fig. 3), with superchondritic Zr/Hf (45.9–47.2) and Ca/Al ratios (1.20–1.22; Fig. 6c). These characteristics are similar to those of low-SiO_2 basalts from Xinchang–Shengzhou, which are considered to represent carbonated peridotite-derived melts (Yu et al., 2015). Such carbonated characteristics can also been certified by the light Mg isotopic compositions of low-SiO_2 basalts from Ninghai and Xinchang–Shengzhou ($\delta^{26}Mg = -0.29$‰ to -0.38‰).

Mg isotopic fractionation during high-temperature processes, e.g., fractional crystallization and partial melting, is limited (e.g., Teng et al., 2007; Zhong et al., 2017). The negative correlation between MgO and δ^{26}Mg for these Zhejiang basalts (not shown) also indicates that light Mg isotopic compositions are not induced by fractional crystallization. Recent studies suggest that low-degree partial melting of garnet-peridotite/pyroxenite may also result in light Mg isotopic compositions, since garnet is enriched in light Mg isotopes compared with other coexisting silicate minerals (Huang et al., 2013; Zhong et al., 2017). However, the difference (~10%) in melting degrees between the Xinchang–Shengzhou basanites/nephelinites and basalts (Supplementary Figure 6; Yu et al., 2015) only causes <0.05‰ difference in δ^{26}Mg (Zhong et al., 2017), which is smaller than the variation observed in samples from this study (0.09‰). Therefore, the involvement of carbonated components in the mantle source is the most likely candidate for explaining the Mg isotopic differences between our samples, which is also considered responsible for the light Mg isotopic compositions of Cenozoic basalts in eastern China(Li et al., 2017; Yang et al., 2012). Good correlations between Ca/Al (or Hf/Hf*) and δ^{26}Mg (Fig. 7a and b) strongly support our proposal of carbonated peridotite as the source of the light Mg isotopic compositions of low-SiO_2 basalts from Ninghai and Xinchang–Shengzhou. However, melts from carbonated components generally have negative Nb and Ta anomalies compared with LREE (e.g., Hoernle et al., 2002), which is different from our samples (Fig. 3). A possible explanation is that carbonated silicate melts are enriched in strongly incompatible elements, and therefore are easy to react with nearby peridotite (Mallik and Dasgupta, 2013). The melt-rock interaction would significantly decrease the abundance of REEs, but with little modification of the HFSEs such as Nb and Ta (Zhang et al., 2017).

5.2.3. Rutile-bearing eclogitic component in the mantle source

High-SiO_2 basalts from Ninghai show similar Sr–Nd–Hf isotopic compositions to low-SiO_2 basalts from Ninghai and Xinchang–Shengzhou(Fig. 4a and b). However, these basalts have positive Ti anomalies (Fig. 3) and their Ti/Ti* ratios (1.03–1.20) correlate with Sr–Nd–Hf isotopic compositions (Fig. 6a and b). Furthermore, the Ninghai high-SiO_2 basalts are also characterized by high $Fe_2O_3^T$ and TiO_2 with moderate MgO contents (Table 1). These observations can hardly be explained by the melting of peridotite (e.g., Takahashi et al., 1993). Hornblendite-derived melts constrained by melting experiments have low $(K_2O + Na_2O)/TiO_2$ values (<1) (Pilet et al., 2008), which differ from the Ninghai high-SiO_2 basalts ($(K_2O + Na_2O)/TiO_2 = 1.2$–$1.6$). Therefore, we infer that eclogite/pyroxenite is a possible source lithology of basalts with depleted isotopic compositions. The Ninghai high-SiO_2 basalts have high Sm/Yb and low Lu/Hf ratios (Fig. 6d), which also indicate the important influence of garnet in the source (because HREEs are strongly compatible in garnet; e.g.,

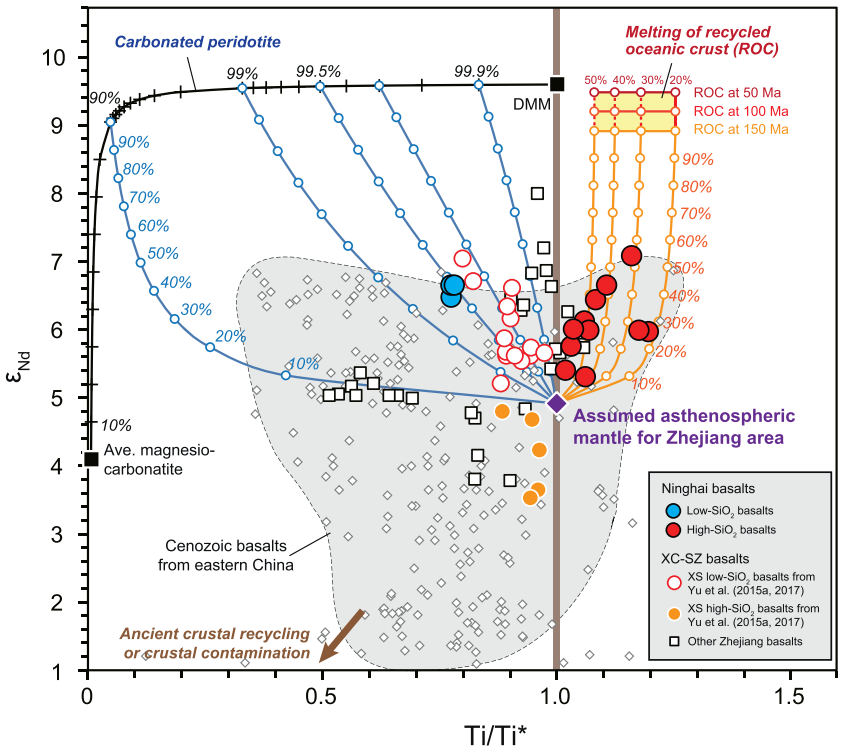

Fig. 8. Variation in ε_{Nd} versus Ti/Ti* values for Ninghai and Xinchang-Shengzhou basalts, their various source components, and invoked mixing relations. We calculated the Nd isotopic composition of recycled oceanic crust at various time by using the present-day average isotopic compositions of Pacific Ocean MORB (http://www.earthchem.org/petdb). The method for calculation can be referred to Chauvel et al. (2008). Melting models were calculated for fractional melting of eclogite (garnet:clinopyroxene = 1:1) with 1% rutile. For carbonated mantle peridotite, we modeled the mixing between DMM (Workman and Hart, 2005) and average igneous carbonatites which are based on data for oceanic magnesio-carbonatite from Cape Verdes (Hoernle et al., 2002). Details of the calculations are given in Supplementary Table4. Data for published Cenozoic basalts from Zhejiang (Ho et al., 2003; Li et al., 2015; Liu et al., 2016b; Zou et al., 2000) and eastern China (see Fig. 4 for detailed reference list) are presented as comparison. For samples from Zhejiang area, only samples with little influence from crustal contamination (Nb/U > 45) and fractional crystallization (MgO > 6 wt%) are picked up for comparison.

Westrenen et al., 1999). In addition, the large variations in TiO_2 contents (Table 1) and positive Ti anomalies (Fig. 6) indicate the presence of rutile-bearing eclogite in the source, since rutile is a common accessory phase in eclogite and Ti is highly compatible in rutile (e.g., Foley et al., 2000; Klemme et al., 2005). Residual rutile in the source would strongly buffer the Ti abundance in melts. Experimental petrology studies have shown that rutile can be consumed at moderate degrees of partial melting (~22%; Gaetani et al., 2008). Additionally, the TiO_2 content of the rutile-bearing eclogitic source would also affect rutile consumption. For example, for an eclogitic source with $TiO_2 \leq 1.6$ wt %, ~25% partial melting can completely consume the rutile at a temperature of 1250 °C (Klemme et al., 2002). If the rutile was totally consumed, the melt would be enriched in Ti and ultimately form basalts with positive Ti anomalies (e.g., Foley et al., 2000; Rudnick et al., 2000), which is similar to the geochemical features of the Ninghai high-SiO_2 basalts. In addition to Ti, Hf is also compatible in rutile (e.g., Klemme et al., 2002, 2005). The positive correlations between Ti/Ti* and Hf/Hf* (not shown) also support the existence of rutile in the source. Furthermore, Ca/Al ratios are negatively correlated with Ti/Ti* ratios (Fig. 6c), indicating that the consumption of rutile, together with residual clinopyroxene, played an important role in the source (because Ca/Al is controlled by clinopyroxene in the source; e.g., Hirschmann et al., 2003; Kogiso et al., 2003). An eclogite component therefore exists in the mantle source for the Ninghai high-SiO_2 basalts, in addition to mantle peridotite. The terrestrial mantle-like Mg isotopic compositions of the Ninghai high-SiO_2 basalts can be explained by high-degree (~15%–20%) partial melting (Yu et al., 2015) of the mixed source of asthenospheric mantle peridotite and rutile-bearing eclogite.

5.3. Recycling of Pacific oceanic crust

Ti-enrichment in OIB indicates that recycled oceanic crust is present in the mantle source (Prytulak and Elliott, 2007). The consistently depleted Sr–Nd–Hf and light Mg isotopic compositions (Fig. 4) of the Ninghai and Xinchang–Shengzhou basalts indicate that they were derived from the same young oceanic crust, rather than from ancient (>1 Ga) crust, as ancient crust generally has more enriched isotopic compositions than young crust (Zeng et al., 2017). Since the Mesozoic, subduction of the Pacific Plate has played an important role in controlling the tectonic evolution of eastern China(Li and Li, 2007) and related basaltic magmatism (e.g., Zeng et al., 2016). Geophysical observations indicate that a stagnant cold and dense component (representing the Pacific oceanic slab) is present in the mantle transition zone (Huang and Zhao, 2006; Liu et al., 2017b). Recycling of Pacific oceanic crust has been considered in studies of intraplate basalts from northeastern and northern China (e.g., Sakuyama et al., 2013; Xu et al., 2012, Xu, 2014), where unusual geochemical features have been observed, such as the positive correlation between $^{87}Sr/^{86}Sr$ and ε_{Nd} in the Shuangliao basalts (Xu et al., 2012). Unlike DMM and Indian Ocean MORB, Pacific Ocean MORB is characterized by decoupled Nd-Hf isotopes that generally plot below the mantle-array line (Fig. 4b). The $\Delta\varepsilon_{Hf}$ value is used to evaluate the degree of decoupling of Hf relative to Nd. Pacific MORB has negative $\Delta\varepsilon_{Hf}$ values, Indian MORB has positive $\Delta\varepsilon_{Hf}$ values, and DMM has values close to unity (Workman and Hart, 2005) (Fig. 7c). The depleted end-member of the Ninghai and Xinchang–Shengzhou samples is characterized by high ε_{Nd} and negative $\Delta\varepsilon_{Hf}$ values, and plots toward the calculated evolutionary path of Pacific oceanic crust at ~200–100 Ma (Fig. 4b). The oldest Pacific oceanic crust in the western

Pacific Ocean formed at ~170 Ma (Koppers et al., 2003). It is therefore suggested that the Pacific oceanic crust should be considered as the source of the recycled carbonated component and rutile-bearing eclogite in the mantle source of the Zhejiang basalts.

5.4. Implications for the petrogenesis of Cenozoic intraplate basalts in eastern China

During the subduction of oceanic slab, CO_2 can be introduced into the mantle transition zone, together with oceanic eclogite, in the form of Mg-rich carbonates (e.g., Dasgupta et al., 2004; Li et al., 2017). Such a carbonated component is unstable at the depth of the mantle transition zone during hot subduction, and likely undergoes partial melting (e.g., Dasgupta et al., 2004; Thomson et al., 2016). The resulting carbonatitic melts then ascend and metasomatize the surrounding mantle peridotite to form carbonated peridotite. This two-stage model can explain the formation of basalts in continental and oceanic environments (e.g., Dasgupta et al., 2007; Hirose, 1997; Li et al., 2017). The geochemical compositions of the Zhejiang basalts provide evidence of both carbonated peridotite and rutile-bearing eclogite in the mantle source. Both components are characterized by similar depleted isotopic compositions, which are consistent with the recycling of subducted Pacific oceanic crust and indicate a genetic relationship between them.

The Pacific oceanic slab underwent cold subduction toward the west (Syracuse et al., 2010), and the subducted carbonated eclogite should therefore be stable in the mantle transition zone (Dasgupta et al., 2004; Thomson et al., 2016), which is also supported by the geophysical observations in this area (Huang and Zhao, 2006). Fracturing and upwelling of the stagnant carbonated oceanic crust may have transported carbonated eclogite into the upper mantle. Upon reaching the solidus line, release of the carbonatitic melts would have occurred, leaving an eclogitic residue (e.g., Dasgupta et al., 2007; Zeng et al., 2017). The generated carbonatitic melts then interacted with peridotite to produce carbonated peridotite. The partial melting of carbonated peridotite at about 300 km depth formed melts with low SiO_2 (similar to the nephelinites and basanites from Ninghai and Xinchang–Shengzhou), while the partial melting of the eclogitic component at about 90 km depth formed melts with high SiO_2 (similar to the Ninghai high-SiO_2 basalts). In our simple melt-extraction model (Fig. 8), high melt fractions (20%–50%) were extracted from the rutile-bearing oceanic crust. Eclogite-derivedhigh-degree melts show high Ti/Ti* values (1.08–1.25) because Ti is compatible in rutile (which is exhausted from the residual solid at >22% partial melting; Gaetani et al., 2008). In contrast, carbonatites are characterized by negative Ti anomalies, and thus low-degree melting of a carbonated source would produce melts with low Ti/Ti* values (0.33–0.83). These two types of partial melts ultimately mixed with nearby peridotite-derived melts to produce the Ninghai high-SiO_2 and low-SiO_2 basalts, respectively. Such model can generally explain the compositional variations of basalts in Zhejiang Province, and even Cenozoic intraplate basalts in eastern China (Fig. 8). Basalts with low Nd isotopic compositions ($\varepsilon_{Nd} < 5$) indicate the influence of recycling of ancient crustal materials or crustal contamination.

As discussed above, the coexistence of carbonated and eclogitic sources may be common in the source of intraplate basalts in eastern China, and the mantle carbonitization in this area can be explained by the recycling of young carbonated oceanic crust. In other words, the formation of carbonated oceanic eclogite during Pacific Plate subduction represents an important mechanism in the recycling of sedimentary carbonates. Compared with the recycled sedimentary carbonates with radiogenic Sr isotopic compositions (Huang and Xiao 2016, and reference therein), the carbonitization of oceanic crust during subduction may induce Mg-isotopic exchange without significantly changing radiogenic isotopic compositions, thereby resulting in depleted carbonated oceanic crust with a light Mg isotopic composition (e.g., Wang et al., 2014). The positive correlation between Mg and Sr isotopic compositions (Fig. 4c) and the negative correlation between Mg and Nd isotopic compositions (Fig. 4d) for the Zhejiang basalts may confirm the above possibility.

6. Conclusion

Intraplate basaltic volcanism in the Ninghai region produced low-SiO_2 (nephelinites and basanites) and high-SiO_2 basalts by partial melting of carbonated peridotite and rutile-bearing eclogite, respectively. Similarities in the isotopic compositions of low-SiO_2 and high-SiO_2 basalts indicate a genetic relationship between them. Depleted Sr, Nd, and Hf isotopic compositions, as well as negative $\Delta\varepsilon_{Hf}$ and light $\delta^{26}Mg$ values, further indicate that their source components originated from the subducted carbonated Pacific oceanic crust.

Acknowledgement

Zhen Liu and Sen-Lin Hu attended the field investigations of this study. Ya-Jun An, Yuan-Xin Xiang, Yue-Heng Yang, Wei Pu, Huan-Ling Lei, Hai-Zhen Wei, Chao Huang and Ye Liu provided technical support. We appreciate the thoughtful and constructive reviews provided by Dr. Andrew Kerr and two anonymous reviewers. This study was supported by the National Natural Science Foundation of China (grants 41672048, 41430208, and 41530964). Xun Yu is sponsored by Shanghai Sailing Program (17YF1420300) and China Postdoctoral Science Foundation (2017M621525).

Appendix A. Supplementary data

Supplementary data to this article can be found online at https://doi.org/10.1016/j.lithos.2018.11.003.

References

An, Y., Wu, F., Xiang, Y., Nan, X., Yu, X., Yang, J., et al., 2014. High-precision Mg isotope analyses of low-Mg rocks by MC-ICP-MS. Chem. Geol. 390, 9–21. https://doi.org/10.1016/j.chemgeo.2014.09.014.

Carlson, R.W., Lugmair, G.W., MacDougall, J.D., 1981. Columbia River volcanism: the question of mantle heterogeneity or crustal contamination. Geochim. Cosmochim. Acta 45, 2483–2499. https://doi.org/10.1016/0016-7037(81)90100-9.

Charvet, J., Shu, L.-S., Shi, Y.-S., Guo, L.-Z., Faure, M., 1996. The building of south China: collision of Yangzi and Cathaysia blocks, problems and tentative answers. J. Southeast Asian Earth Sci. 13, 223–235. https://doi.org/10.1016/0743-9547(96)00029-3.

Chauvel, C., Lewin, E., Carpentier, M., Arndt, N.T., Marini, J.-C., 2008. Role of recycled oceanic basalt and sediment in generating the Hf-Nd mantle array. Nat. Geosci. 1, 64–67.

Chen, J., Jahn, B.-M., 1998. Crustal evolution of southeastern China: Nd and Sr isotopic evidence. Tectonophysics 284, 101–133. https://doi.org/10.1016/S0040-1951(97)00186-8.

Chen, L.H., Zeng, G., Jiang, S.Y., Hofmann, A.W., Xu, X.S., Pan, M.B., 2009. Sources of Anfengshan basalts: Subducted lower crust in the Sulu UHP belt, China. Earth Planet. Sci. Lett. 286, 426–435. https://doi.org/10.1016/j.epsl.2009.07.006.

Chen, H., Xia, Q.-K., Ingrin, J., Deloule, E., Bi, Y., 2016. Heterogeneous source components of intraplate basalts from NEChina induced by the ongoing Pacific slab subduction. Earth Planet. Sci. Lett. 459, 208–220. https://doi.org/10.1016/j.epsl.2016.11.030.

Danyushevsky, L.V., Plechov, P., 2011. Petrolog 3: Integrated software for modeling crystallization processes. Geochem. Geophys. Geosyst. 12, 785–814. https://doi.org/10.1029/2011GC003516.

Dasgupta, R., Hirschmann, M.M., Withers, A.C., 2004. Deep global cycling of carbon constrained by the solidus of anhydrous, carbonated eclogite under upper mantle conditions. Earth Planet. Sci. Lett. 227, 73–85. https://doi.org/10.1016/j.epsl.2004.08.004.

Dasgupta, R., Hirschmann, M.M., Smith, N.D., 2007. Partial melting experiments of peridotite + CO_2 at 3 GPa and genesis of alkalic Ocean Island Basalts. J. Petrol. 48, 2093–2124. https://doi.org/10.1093/petrology/egm053.

Fan, Q.C., Chen, S.S., Zhao, Y.W., Zou, H.B., Li, N., Sui, J.L., 2014. Petrogenesis and evolution of Quaternary basaltic rocks from the Wulanhada area, North China. Lithos 206-207, 289–302.

Foley, S.F., Barth, M.G., Jenner, G.A., 2000. Rutile/melt partition coefficients for trace elements and an assessment of the influence of rutile on the trace element characteristics of subduction zone magmas. Geochim. Cosmochim. Acta 64, 933–938. https://doi.org/10.1016/S0016-7037(99)00355-5.

Gaetani, G.A., Asimow, P.D., Stolper, E.D., 2008. A model for rutile saturation in silicate melts with applications to eclogite partial melting in subduction zones and mantle plumes. Earth Planet. Sci. Lett. 272 (3–4).

Galy, A., Yoffe, O., Janney, P.E., Williams, R.W., Cloquet, C., Alard, O., et al., 2003. Magnesium isotope heterogeneity of the isotopic standard SRM980 and new reference materials for magnesium-isotope-ratio measurements. J. Anal. At. Spectrom. 18, 1352–1356. https://doi.org/10.1039/B309273A.

Gerbode, C., Dasgupta, R., 2010. Carbonate-fluxed melting of MORB-like pyroxenite at 2.9 GPa and genesis of HIMU Ocean island basalts. J. Petrol. 51, 2067–2088. https://doi.org/10.1093/petrology/egq049.

Guo, P., Niu, Y., Sun, P., Ye, L., Liu, J., Zhang, Y., Feng, Y.-X., Zhao, J.-X., 2016. The origin of Cenozoic basalts from central Inner Mongolia, East China: the consequence of recent mantle metasomatism genetically associated with seismically observed paleo-Pacific slab in the mantle transition zone. Lithos 240–243, 104–118.

Hirose, K., 1997. Partial melt compositions of carbonated peridotite at 3 GPa and role of CO2 in alkali-basalt magma generation. Geophys. Res. Lett. 24, 2837–2840. https://doi.org/10.1029/97GL02956.

Hirschmann, M.M., Kogiso, T., Baker, M.B., Stolper, E.M., 2003. Alkalic magmas generated by partial melting of garnet pyroxenite. Geology 31, 481–484.

Ho, K.-S., Chen, J.-C., Lo, C.-H., Zhao, H.-L., 2003. ^{40}Ar–^{39}Ar dating and geochemical characteristics of late Cenozoic basaltic rocks from the Zhejiang–Fujian region, SEChina: eruption ages, magma evolution and petrogenesis. Chem. Geol. 197, 287–318. https://doi.org/10.1016/S0009-2541(02)00399-6.

Hoernle, K., Tilton, G., Le Bas, M.J., Duggen, S., Garbe-Schönberg, D., 2002. Geochemistry of oceanic carbonatites compared with continental carbonatites: mantle recycling of oceanic crustal carbonate. Contrib. Mineral. Petrol. 142, 520–542. https://doi.org/10.1007/s004100100308.

Hofmann, A.W., Jochum, K.P., Seufert, M., White, W.M., 1986. Nb and Pb in oceanic basalts: new constraints on mantle evolution. Earth Planet. Sci. Lett. 79, 33–45. https://doi.org/10.1016/0012-821X(86)90038-5.

Huang, J., Xiao, Y., 2016. Mg-Sr isotopes of low-$\delta^{26}Mg$ basalts tracing recycled carbonate species: Implication for the initial melting depth of the carbonated mantle in Eastern China. Int. Geol. Rev. 58, 1350–1362. https://doi.org/10.1080/00206814.2016.1157709.

Huang, J.-L., Zhao, D.-P., 2006. High-resolution mantle tomography of China and surrounding regions. J. Geophys. Res. Solid Earth (1978–2012), 111 https://doi.org/10.1029/2005JB004066.

Huang, F., Chen, L., Wu, Z., Wang, W., 2013. First-principles calculations of equilibrium Mg isotope fractionations between garnet, clinopyroxene, orthopyroxene, and olivine: implications for Mg isotope thermometry. Earth Planet. Sci. Lett. 367, 61–70. https://doi.org/10.1016/j.epsl.2013.02.025.

Huang, J., Li, S.G., Xiao, Y.L., Ke, S., Li, W.Y., Tian, Y., 2015. Origin of low $\delta^{26}Mg$ Cenozoic basalts from South China Block and their geodynamic implications. Geochim Cosmochim Acta 164, 298–317.

Irifune, T., Ringwood, A.E., Hibberson, W.O., 1994. Subduction of continental crust and terrigenous and pelagic sediments: an experimental study. Earth Planet. Sci. Lett. 126, 351–368.

Jackson, M.G., Price, A.A., Blichert-Toft, J., Kurz, M.D., Reinhard, A.A., 2017. Geochemistry of lavas from the Caroline hotspot, Micronesia: evidence for primitive and recycled components in the mantle sources of lavas with moderately elevated $^{3}He/^{4}He$. Chem. Geol. 455, 385–400. https://doi.org/10.1016/j.chemgeo.2016.10.038.

Jochum, K.P., Weis, U., Schwager, B., Stoll, B., Wilson, S.A., Haug, G.H., Andreae, M.O., Enzweiler, J., 2016. Reference values following ISO guidelines for frequently requested rock reference materials. 40, 333–350.

Johnson, K.T.M., 1998. Experimental determination of partition coefficients for rare earth and high-field-strength elements between clinopyroxene, garnet, and basaltic melt at high pressures. Contrib. Mineral. Petrol. 133, 60–68.

Klemme, S., Blundy, J.D., Wood, B.J., 2002. Experimental constraints on major and trace element partitioning during partial melting of eclogite. Geochim. Cosmochim. Acta 66, 3109–3123.

Klemme, S., Prowatke, S., Hametner, K., Günther, D., 2005. Partitioning of trace elements between rutile and silicate melts: Implications for subduction zones. Geochim. Cosmochim. Acta 69, 2361–2371. https://doi.org/10.1016/j.gca.2004.11.015.

Kogiso, T., Hirschmann, M.M., Frost, D.J., 2003. High-pressure partial melting of garnet pyroxenite: possible mafic lithologies in the source of ocean island basalts. Earth Planet. Sci. Lett. 216, 603–617. https://doi.org/10.1016/S0012-821X(03)00538-7.

Koppers, A.A.P., Staudigel, H., Duncan, R.A., 2003. High-resolution$^{40}Ar/^{39}Ar$ dating of the oldest oceanic basement basalts in the western Pacific basin. Geochem. Geophys. Geosyst. 4. https://doi.org/10.1029/2003GC000574.

Kumar, K.V., Chavan, C., Sawant, S., Raju, K.N., Kanakdande, P., Patode, S., et al., 2010. Geochemical investigation of a semi-continuous extrusive basaltic section from the Deccan Volcanic Province, India: implications for the mantle and magma chamber processes. Contrib. Mineral. Petrol. 159, 839–862.

Kuritani, T., Ohtani, E., Kimura, J.-I., 2011. Intensive hydration of the mantle transition zone beneath China caused by ancient slab stagnation. Nat. Geosci. https://doi.org/10.1038/NGEO1250.

Lai, Y.J., Von Strandmann, P.A.E.P., Dohmen, R., Takazawa, E., Elliott, T., 2015. The influence of melt infiltration on the Li and Mg isotopic composition of the Horoman Peridotite Massif. Geochim. Cosmochim. Acta 164, 318–332. https://doi.org/10.1016/j.gca.2015.05.006.

Le Bas, M.J., Le Maitre, R.W., Streckeisen, A., Zanettin, B., 1986. A chemical classification of volcanic rocks based on the total alkali-silica diagram. J. Petrol. 27, 745–750. https://doi.org/10.1093/petrology/27.3.745.

Li, Z.X., Li, X.H., 2007. Formation of the 1300-km-wide intracontinental orogen and postorogenic magmatic province in Mesozoic South China: a flat-slab subduction model. Geology 35, 179–182.

Li, Y.-Q., Ma, C.-Q., Robinson, P.T., Zhou, Q., Liu, M.-L., 2015. Recycling of oceanic crust from a stagnant slab in the mantle transition zone: evidence from Cenozoic continental basalts in Zhejiang Province, SEChina. Lithos 230, 146–165. https://doi.org/10.1016/j.lithos.2015.05.021.

Li, Y.Q., Ma, C.Q., Robinson, P.T., Zhou, Q., Liu, M.L., 2015. Recycling of oceanic crust from a stagnant slab in the mantle transition zone: evidence from Cenozoic continental basalts in Zhejiang Province, SE China. Lithos 230, 146–165.

Li, H.Y., Xu, Y.G., Ryan, J.G., Huang, X.L., Ren, Z.Y., Guo, H., Ning, Z.G., 2016. Olivine and melt inclusion chemical constraints on the source of intracontinental basalts from the eastern North China Craton: Discrimination of contributions from the subducted Pacific slab. Geochim Cosmochim Acta 178, 1–19.

Li, Y.Q., Ma, C.Q., Robinson, P.T., 2016. Petrology and geochemistry of Cenozoic intra-plate basalts in east-central China: constraints on recycling of an oceanic slab in the source region. Lithos 262, 27–43.

Li, S.-G., Yang, W., Ke, S., Meng, X., Tian, H., Xu, L., et al., 2017. Deep carbon cycles constrained by a large-scale mantle Mg isotope anomaly in eastern China. Nat. Sci. Rev. 4, 111–120. https://doi.org/10.1093/nsr/nww070.

Liu, R.X., Chen, W.J., Sun, J.Z., Li, D.M., 1992. The K–Ar age and tectonic environment of Cenozoic volcanic rocks in China. Seismology Publ, Beijing, pp. 1–43 In Chinese.

Liu, J., Xia, Q.-K., Deloule, E., Chen, H., Feng, M., 2015. Recycled oceanic crust and marine sediment in the source of alkali basalts in Shandong, eastern China: evidence from magma water content and oxygen isotopes. J. Geophys. Res. Solid Earth 120 (12), 8281–8303.

Liu, S.A., Wang, Z.Z., Li, S.G., Huang, J., Yang, W., 2016a. Zinc isotope evidence for a large-scale carbonated mantle beneath eastern China. Earth Planet. Sci. Lett. 444, 169–178.

Liu, S.C., Xia, Q.K., Choi, S.H., Deloule, E., Li, P., Liu, J., 2016b. Continuous supply of recycled Pacific oceanic materials in the source of Cenozoic basalts in SEChina: the Zhejiang case. Contrib. Mineral. Petrol. 171 (100). https://doi.org/10.1007/s00410-016-1310-4.

Liu, J.-Q., Chen, L.-H., Wang, X.-J., Zhong, Y., Yu, X., Zeng, G., Erdmann, S., 2017a. The role of melt-rock interaction in the formation of Quaternary high-MgO potassic basalt from the Greater Khingan Range, Northeast China. J. Geophys. Res. Solid Earth 122. https://doi.org/10.1002/2016JB013605.

Liu, X., Zhao, D., Li, S., Wei, W., 2017b. Age of the subducting Pacific slab beneath East Asia and its geodynamic implications. Earth Planet. Sci. Lett. 464, 166–174.

Mallik, A., Dasgupta, R., 2013. Reactive infiltration of MORB-eclogite-derived carbonated silicate melt into fertile peridotite at 3 GPa and genesis of alkali magmas. J. Petrol. 54, 2267–2300.

McDonough, W.F., Sun, S.-S., 1995. The composition of the Earth. Chem. Geol. 120, 223–253. https://doi.org/10.1016/0009-2541(94)00140-4.

Pilet, S., Baker, M.B., Stolper, E.M., 2008. Metasomatized lithosphere and the origin of alkaline lavas. Science 320, 916–919. https://doi.org/10.1126/science.1156563.

Prytulak, J., Elliott, T., 2007. TiO_2 enrichment in ocean island basalts. Earth Planet. Sci. Lett. 263, 388–403.

Rudnick, R.L., Gao, S., 2014. Composition of the Continental Crust. In: Turekian, H.D.H.K. (Ed.), Treatise on Geochemistry, second edition Elsevier, Oxford, pp. 1–51.

Rudnick, R.L., Barth, M., Horn, I., McDonough, W.F., 2000. Rutile-bearing refractory eclogites: missing link between continents and depleted mantle. Science 287, 278–281. https://doi.org/10.1126/science.287.5451.278.

Sakuyama, T., Tian, W., Kimura, J.-I., Fukao, Y., Hirahara, Y., Takahashi, T., et al., 2013. Melting of dehydrated oceanic crust from the stagnant slab and of the hydrated mantle transition zone: constraints from Cenozoic alkaline basalts in eastern China. Chem. Geol. 359, 32–48. https://doi.org/10.1016/j.chemgeo.2013.09.012.

Sobolev, A.V., Hofmann, A.W., Sobolev, S.V., Nikogosian, I.K., 2005. An olivine-free mantle source of Hawaiian shield basalts. Nature 434, 590–597. https://doi.org/10.1038/nature03411.

Sun, Y., Teng, F.Z., Ying, J.F., Su, B.X., Hu, Y., Fan, Q.C., Zhou, X.H., 2017. Magnesium isotopic evidence for ancient subducted oceanic crust in LOMU-likepotassium-rich volcanic rocks. J. Geophys. Res. Solid Earth 122, 7562–7572.

Syracuse, E.M., Keken, P.E.V., Abers, G.A., 2010. The global range of subduction zone thermal models. Phys. Earth Planet. Inter. 183, 73–90. https://doi.org/10.1016/j.pepi.2010.02.004.

Takahashi, E., Shimazaki, T., Tsuzaki, Y., Yoshida, H., 1993. Melting study of a peridotite KLB-1 to 6.5 GPa, and the origin of basaltic magmas. Philos. Trans. R. Soc. London Ser. A 342, 105–120.

Teng, F.-Z., 2017. Magnesium isotope geochemistry. Rev. Mineral. Geochem. 82, 219–287. https://doi.org/10.2138/rmg.2017.82.7.

Teng, F.-Z., Wadhwa, M., Helz, R.T., 2007. Investigation of magnesium isotope fractionation during basalt differentiation: implications for a chondritic composition of the terrestrial mantle. Earth Planet. Sci. Lett. 261, 84–92.

Thomson, A.R., Walter, M.J., Kohn, S.C., Brooker, R.A., 2016. Slab melting as a barrier to deep carbon subduction. Nature 529, 76. https://doi.org/10.1038/nature16174.

Vervoort, J.D., Patchett, P.J., Blichert-Toft, J., Albarède, F., 1999. Relationships between Lu–Hf and Sm–Nd isotopic systems in the global sedimentary system. Earth Planet. Sci. Lett. 168, 79–99. https://doi.org/10.1016/S0012-821X(99)00047-3.

Vervoort, J.D., Plank, T., Prytulak, J., 2011. The Hf-Nd isotopic composition of marine sediments. Geochim. Cosmochim. Acta 75, 5903–5926. https://doi.org/10.1016/j.gca.2011.07.046.

Wang, Y., Zhao, Z.-F., Zheng, Y.-F., Zhang, J.-J., 2011. Geochemical constraints on the nature of mantle source for Cenozoic continental basalts in east-central China. Lithos 125 (3-4), 940–955.

Wang, S.J., Teng, F.Z., Li, S.G., 2014. Tracing carbonate-silicate interaction during subduction using magnesium and oxygen isotopes. Nat. Commun. 5 (5328). https://doi.org/10.1038/ncomms6328.

Wang, X., Wilde, S.A., Li, Q., Yang, Y., 2015. Continental flood basalts derived from the hydrous mantle transition zone. Nat Commun 6 (1), 7700. https://doi.org/10.1038/ncomms8700.

Wang, X.J., Chen, L.H., Hofmann, A.W., Mao, F.G., Liu, J.Q., Zhong, Y., Xie, L.W., Yang, Y.H., 2017. Mantle transition zone-derived EM1 component beneath NE China: Geochemical evidence from Cenozoic potassic basalts. Earth. Planet. Sci. Lett. 465, 16–28.

Weis, D., Kieffer, B., Maerschalk, C., Barling, J., De Jong, J., Williams, G.A., et al., 2006. High-precision isotopic characterization of USGS reference materials by TIMS and MC-ICP-MS. Geochem. Geophys. Geosyst. 7. https://doi.org/10.1029/2006GC001283.

Wang, X.J., Chen, L.H., Hofmann, A.W., Hanyu, T., Kawabata, H., Zhong, Y., Xie, L.W., Shi, J. H., Miyazaki, T., Hirahara, Y., Takahashi, T., Senda, R., Chang, Q., Vaglarov, B.S., Kimura, J.I., 2018. Recycled ancient ghost carbonate in the Pitcairn mantle plume. Proc Natl Acad Sci USA 115 (35), 8682–8687.

Weis, D., Kieffer, B., Hanano, D., Silva, I.N., Barling, J., Pretorius, W., Maerschalk, C., Mattielli, N., 2007. Hf isotope compositions of U.S. Geological Survey reference materials. Geochem. Geophys. Geosyst. 8, 57–77. https://doi.org/10.1029/2006GC0011473.

Westrenen, W.v., Blundy, J., Wood, B., 1999. Crystal-chemical controls on trace element partitioning between garnet and anhydrous silicate melt. Am. Mineral. 84, 838–847.

Workman, R.K., Hart, S.R., 2005. Major and trace element composition of the depleted MORB mantle (DMM). Earth Planet. Sci. Lett. 231, 53–72. https://doi.org/10.1016/j.epsl.2004.12.005.

Xu, Y.-G., 2014. Recycled oceanic crust in the source of 90-40 Ma basalts in North and Northeast China: evidence, provenance and significance. Geochim. Cosmochim. Acta 143, 49–67. https://doi.org/10.1016/j.gca.2014.04.045.

Xu, Y.-G., Zhang, H.-H., Qiu, H.-N., Ge, W.-C., Wu, F.-Y., 2012. Oceanic crust components in continental basalts from Shuangliao, Northeast China: Derived from the mantle transition zone? Chem. Geol. 328, 168–184. https://doi.org/10.1016/j.chemgeo.2012.01.027.

Xu, Z., Xu, Z., Zhao, Z.F., Zheng, Y.F., 2012. Slab–mantle interaction for thinning of cratonic lithospheric mantle in North China: geochemical evidence from Cenozoic continental basalts in central Shandong. Lithos 146–147, 202–217.

Xu, R., Liu, Y., Wang, X., Zong, K., Hu, Z., Chen, H., Zhou, L., 2017. Crust recycling induced compositional-temporal-spatial variations of Cenozoic basalts in the Trans-North China Orogen. Lithos 274-275, 383–396.

Yang, Y.-H., Zhang, H.-F., Chu, Z.-Y., Xie, L.-W., Wu, F.-Y., 2010. Combined chemical separation of Lu, Hf, Rb, Sr, Sm and Nd from a single rock digest and precise and accurate isotope determinations of Lu–Hf, Rb–Sr and Sm–Nd isotope systems using Multi-CollectorICP-MS and TIMS. Int. J. Mass Spectrom. 290, 120–126.

Yang, W., Teng, F.-Z., Zhang, H.-F., Li, S.-G., 2012. Magnesium isotopic systematics of continental basalts from the North China craton:Implications for tracing subducted carbonate in the mantle. Chem. Geol. 328, 185–194.

Yarmolyuk, V.V., Kudryashova, E.A., Kozlovsky, A.M., Lebedev, V.A., Savatenkov, V.M., 2015. Late Mesozoic–Cenozoic intraplate magmatism in Central Asia and its relation with mantle diapirism: evidence from the South Khangai volcanic region, Mongolia. J Asian Earth Sci 111, 604–623.

Yaxley, G.M., 2000. Experimental study of the phase and melting relations of homogeneous basalt+peridotite mixtures and implications for the petrogenesis of flood basalts. Contrib. Mineral. Petrol. 139, 326–338.

Young, E.D., Galy, A., 2004. The isotope geochemistry and cosmochemistry of Magnesium. Rev. Mineral. Geochem. 55, 197–230.

Yu, X., Chen, L.-H., Zeng, G., 2015. Growing magma chambers control the distribution of small-scale flood basalts. Sci. Rep. 5 (16824). https://doi.org/10.1038/srep16824.

Yu, X., Chen, L.-H., Zeng, G., 2017. Magmatic recharge buffers the isotopic compositions against crustal contamination in formation of continental flood basalts. Lithos 284-285, 1–10. https://doi.org/10.1016/j.lithos.2017.03/027.

Zeng, G., Chen, L.-H., Xu, X.-S., Jiang, S.-Y., Hofmann, A.W., 2010. Carbonated mantle sources for Cenozoic intra-plate alkaline basalts in Shandong, North China. Chem. Geol. 273, 35–45. https://doi.org/10.1016/j.chemgeo.2010.02.009.

Zeng, G., He, Z.-Y., Li, Z., Xu, X.-S., Chen, L.-H., 2016. Geodynamics of paleo-Pacific plate subduction constrained by the source lithologies of late Mesozoic basalts in southeastern China. Geophys. Res. Lett. 43, 10189–10197. https://doi.org/10.1002/2016GL070346.

Zeng, G., Chen, L.-H., Yu, X., Liu, J.-Q., Xu, X.-S., Erdmann, S., 2017. Magma-magma interaction in the mantle beneath eastern China. J. Geophys. Res. Solid Earth 122, 2763–2769. https://doi.org/10.1002/2017JB014023.

Zhang, M., Guo, Z., 2016. Origin of late Cenozoic Abaga-Dalinuoer basalts, eastern China: implications for a mixed pyroxenite-peridotite source related with deep subduction of the Pacific slab. Gondwana Res. 37, 130–151.

Zhang, J.-J., Zheng, Y.-F., Zhao, Z.-F., 2009. Geochemical evidence for interaction between oceanic crust and lithospheric mantle in the origin of Cenozoic continental basalts in east-central China. Lithos 110, 305–326. https://doi.org/10.1016/j.lithos.2009.01.006.

Zhang, G.L., Chen, L.H., Jackson, M.G., Hofmann, A., 2017. Evolution of carbonated melt to alkali basalt in the South China Sea. Nat. Geosci. https://doi.org/10.1038/NGEO2877.

Zhong, Y., Chen, L.-H., Wang, X.-J., Zhang, G.-L., Xie, L.-W., Zeng, G., 2017. Magnesium isotopic variation of oceanic island basalts generated by partial melting and crustal recycling. Earth Planet. Sci. Lett. 463, 127–135. https://doi.org/10.1016/j.epsl.2017.01.040.

Zou, H.-B., Zindler, A., Xu, X.-S., Qi, Q., 2000. Major, trace element, and Nd, Sr and Pb isotope studies of Cenozoic basalts in SEChina: mantle sources, regional variations, and tectonic significance. Chem. Geol. 171, 33–47. https://doi.org/10.1016/S0009-2541(00)00243-6.